Abstract

Our research is one part of the “Innovative Aerial Robot Project” (IARP) is a project for Unmanned Aerial Vehicle (UAV) and Micro Aerial Vehicle (MAV) which is carried out as part of the 21st century centers of excellence (COE) program, “Mechanical Systems Innovation”. “Innovative” means that MAV contains some challenging technologies. In this project, we plan to transmit microwave energy for MAV by phased array antenna, tracking system and polarity-free rectenna.

In this paper, development status of improving rectifier and rectenna array to move motor of MAV with using that system is presented. Firstly, I reviewed the parameter of the rectifier circuit, and I choose that have made improve the best value from the experiment result. The quality of rectifier used in this rectennas array came to be able to convert input-RF into output-DC at the maximum 49% in the 700mW input. Secondly, to obtain the energy beam efficiency, by making the antennas-intensive parallel array. In the 82cm this energy field, I developed the rectennas array with the maximum conversion efficiency of 33% at the load resistance of 260Ω to be match the motor of MAV. Lastly, I established the system by synchronized the motor of rotating MAV with the steering power transmission energy from horn antenna. The high conversion efficiency of renctennas array made that possible.

In this experiment, we have constructed microwave transmission system. The microwave is provided by a 5.8GHz Field Effect Transistor (FET) microwave oscillator (Almotech Co.) and divided into five elements using a power divider. The phases of the microwave elements are controlled individually using two 6-bit phase shifters, whose phase resolution is 5.6deg. The phase shifters were controlled by a PC digitally. Three FET amplifiers with the output power of 0.7 watt each are used to have totally 3.5 watts output power. Each microwave is guided to each antenna. In this experiment, horn antenna is used in order to cut down the number of antenna. The power profile was obtained using a patch antenna connected with rectifier (Pasternack Co.) on a traverse stage.

Acknowledgements

I would like to express his sincerest gratitude to my advisor, Associate Professor Kimiya Komurasaki (Department of Advanced Energy, University of Tokyo) for his continuous and attentive guidance, support, discussion, and encouragement.

I would like to express my thanks to Professor Yoshihiro Arakawa (Department of Aeronautics and Astronautics, University of Tokyo) for his insightful advices.

I would like to express my gratitude to the members of Komurasaki Laboratory and Arakawa Laboratory for their intellectual and social contributions. Mr. Oda, Mr. Takayanagi, Mr. Ozawa, Mr. Katsunaga Ms. Shimane and Mr. Komaru helped me while studying about the microwave power transmission together. Mr. Yokota gave me a lot of precious advice.

I am grateful to Associate Professor Naoki Shinohara (Research Institute for Sustainable Humanosphere, University of Kyoto) for his advice about the microwave power transmission.

Without any of support, this thesis would not have been completed. Thank you.

Finally, I gave my special thanks to my parents for their money and mental support throughout my education.

Contents

Abstract · · ·

3.4 Theory of Polarity-Free Antenna ・・・

Chapter 5
Experiment Results and Discussion

5.1 Rectifier circuit design67
5.1.1 Schematic of the rectifier circuit · 67
5.1.2 Experiment method · 70
5.1.3 Stub Length: l_s · 71
5.1.4 Low Pass Filter: W_C and l_C · 72
5.1.5 Capacitance of Chip Condenser: C_0 · 73
5.1.6 Efficiency of New Rectifier Circuit · 74
5.2 Rectennas Array · 76
5.2.2 Making series and parallel array · 77
5.2.3 Making Parallel Rectennas Array Consolidate and Compact · · · · · · · · · · 78
5.2.4 Making New Rectennas Array · 80
5.3 Demonstration · 82
5.3.1 Beam steering · 82
5.3.2 Beam synchronized with MAV · 82

Chapter 6
Conclusions

6.1. Conclusions · 84
6.2. Future vision · 84

Reference

List of Figures

Figure 1.1 Imaginary picture
Figure 1.2 Schematic of issues
Figure 1.3 Schematic of target tracking system
Figure 1.4 Block Diagram of Tracking System
Figure 1.5 Schematic of Beam Steering by Phased Array Antennas
Figure 1.6 E_y Distribution at h=1m
Figure 1.7 Computed Main-lobe Fractional Energy and Beam Divergence Angle
Figure 1.8 Rectifier Circuit
Figure 1.9 Parallel Rectennas Circuit
Figure 2.1 Simple model of two wave sources
Figure 2.2 Relation of incident wave and phase difference
Figure 2.3 Aperture of rectangular waveguide
Figure 2.4 Horn antenna
Figure 2.5 Electric and Magnetic unit currents
Figure 2.6 Transmitting antennas array
Figure 2.7 Block diagram of the transmission system with three antennas
Figure 2.8 Block diagram of the transmission system with five antennas
Figure 2.9 Phase shifting signal input form
Figure 2.10 Measured radiation field from one horn antenna in the xy-plane
Figure 2.11 Measured radiation fields from one horn antenna with the parameter of height
Figure 2.12 Comparison of measured and calculated field from one horn antenna with the parameter of the height
Figure 2.13 Comparison of measured and calculated 3-dB width
Figure 2.14 Radiation fields from one-dimensional antenna array with the phase-shift control
Figure 2.15 Comparison of measured and calculated radiation field from one-dimensional antenna array at 1020 mm
Figure 2.16 Comparison of measured and calculated radiation field from two-dimensional antenna array at 1040 mm
Figure 2.17 Simulated radiation fields from three types of antenna arrays at 1040 mm high. The plot is represented in the xy-plane

Figure 2.18 Beam diameter
Figure 3.1 Schematic of Rectenna
Figure 3.2 RF-DC Conversion Efficiency of Rectenn
Figure 3.3 Feeding Methods of MSA Element
Figure 3.4 Rectanglar MSA and its Coordinate System
Figure 3.5 Schematic of Electromagnetic Distribution of TM_{100} wave
Figure 3.6 Simple Schematic of Rectifier Circuit with Input and Output Filters
Figure 3.7 Schematic of Rectifier Circuit with Lumped-element Input and Output Filters
Figure 3.8 Schematic of Rectifier Circuit with a Transmission Line as Output Filter
Figure 3.9 Rectifier Circuit Pattern
Figure 3.10 Schematic of Rectifier Circuit for Experiment
Figure 3.11 Structure of Micro-Strip Line
Figure 3.12 Pattern and Equivalent Circuit of Micro-Strip Stub
Figure 3.13 Relationship between DC equivalent circuit and load-line
Figure 3.14 V-I Characteristic of Diode
Figure 3.15 Equivalent Circuit of Diode
Figure 3.16 Detailed Schematic of Rectifier Circuit for Experiment
Figure 3.17 Schematic of Planar wave (TEM) Propagation
Figure 3.18 Schematic of Rotating Polarization Plane
Figure 3.19 Pattern of Unit of Multiple Dipole Antenna
Figure 3.20 Pattern of Patch Antenna for Circular Polarized Wave
Figure 4.1 System overview
Figure 4.2 Oscillator
Figure 4.3 Power divider
Figure 4.4 Digital phase-shifter
Figure 4.5 Driver amplifier
Figure 4.6 Power amplifier
Figure 4.7 Booster amplifier
Figure 4.8 Horn antenna
Figure 4.9 Schematic of Power Receiving System
Figure 4.10 Picture of Patch Antenna
Figure 4.11 Picture of Rectifier
Figure 4.12 Characteristic of Rectifier
Figure 4.13 Picture of Open/Load Switching Unit
Figure 4.14 Schematics of Load/Open Switching Unit
Figure 4.15 Pictures of Oscilloscopes

Figure 4.16 Attenuator
Figure 4.17 Power Meter
Figure 4.18 Polarity-Free Leaf-Patch antenna
Figure 4.19 Picture of Mounting Structure
Figure 4.20 Picture of Electrical Motor
Figure 4.21 Fixed base for demonstration
Figure 4.22 Schematic of demonstration method
Figure 5.1 Schematic of Rectifier Circuit
Figure 5.2 Diagram of the experiment method
Figure 5.3 Relationship between Stub Length and Output Voltage
Figure 5.4 Load Characteristic related to LPF shape
Figure 5.5 Conversion of efficiency
Figure 5.6 Contour map of the rectification efficiency
Figure 5.7 The mesurement method diagram
Figure 5.8 Conversion of efficiency, Rectifier and Rectenna
Figure 5.9 The mesurement method diagram
Figure 5.10 Energy intensive of rectennas
Figure 5.11 Arrangement of recntennas
Figure 5.12 New rectennas array
Figure 5.13 Beam diameter and input power
Figure 5.14 Conversion efficiency and output voltage
Figure 5.15 Characteristic of new rectennas array, 82cm from horn antenna
Figure 5.16 Y-axis output voltage per 1 round
Figure 5.17 X-axis output voltage per 1 round
Figure 5.18 Synchronized result of the output voltage per 1 round

List of Tables

Table.2.1 Port assignment to each phase shifter
Table.4.1 Specifications of Phased Array Antenna
Table.4.2 Specifications of Oscilloscopes
Table.4.3 Specifications of Polarity-Free MSA
Table.4.4 Specification of Substratum
Table.4.5 Specification of Electrical Motor
Table.5.1 Parameters for Standard Rectifier Circuit Pattern
Table.5.2 Efficiency of Chip Condenser
Table.5.3 New Rectifier Parameters
Table.5.4 Efficiency of series and parallel array
Table.5.5 Energy rate of increase

References

[1] 平田 仁, “マイクロ波工学の基礎,” 日本理工出版会, Feb. 2004.

[2] 小澤 亮二, “マイクロ波エネルギー伝送における移相制御と指向性,” 学士論文, 東京大学, Feb. 2005.

[3] 小澤 亮二, “マイクロ波エネルギー伝送システムの開発”, 修士論文, 東京大学, Feb. 2007.

[4] 勝永 健太, “マイクロ飛行機搭載用非偏波方向依存レクテナの開発”, 修士論文, 東京大学, Feb. 2007.

[5] Berndie Strassner, Kai Chang, ”5.8-GHz Circularly Polarized Rectifying Antenna forWireless Microwave Power Transmission” IEEE Transactions on Microwave Theory and Techniques, Vol.50, No.8, Aug.2002

[6] Yong-Chae Jeong, Jong-Sik Lim, ”A Novel Frequency Doubler Using Feedforward Techique and Defected Ground Structure”, IEEE Microwave and Wireless Components Letters, Vol.14, No.12, Dec.2004

[7] 三浦 健史, 篠原 真毅, 松本 紘, “マイクロ波電力伝送用レクテナ素子の接続法に関する実験的研究,” 電子情報通信学会論文誌 B, Vol. J82-B, No.7, pp.1374-1383, Jul. 1999.

[8] R. Ozawa, “Development of Microwave Energy Supply System,” Master thesis, University of Tokyo, Feb. 2007.

[9] 小暮 裕明, “電磁界シミュレータで学ぶ ワイヤレスの世界,” CQ 出版社, Jun. 2001.

[10] T. Yoo and K. Chang, “Theoretical and Experimental Development of 10 and 35 GHz Rectennas,” IEEE Trans. Microwave Theory and Tech., Vol.40, No.6, Jun. 1992.

[11] “アンテナハンドブック,” CQ 出版社 , Feb. 1985.

[12] B. Strassner and K. Chang, “5.8-GHz Circularly Polarized Rectifying Antenna for Wireless Microwave Power Transmission,” IEEE Trans. Microwave Theory and Tech., Vol. 50, pp. 1870-1876, Aug. 2002.

[13] 後藤 尚久, “図説・アンテナ,” (社)電子情報通信学会, Mar. 1995.

[14] 阿部 英太郎, “マイクロ波,” 東京大学出版会, Mar. 1983.

[15] http://www.icom.co.jp/beacon/technical/antenna/005.html

[16] 羽石 操, 平澤 一紘, 鈴木 康夫, “小型・平面アンテナ,” (社)電子情報通信学会, Aug. 1996.

[17] R. J. Gutmann and J. M. Borrego, “Power Combining in an Array of Microwave Power Rectifiers,” IEEE Trans. Microwave Theory and Tech., Vol. MTT-27, pp. 958-968, Dec. 1979.

[18] R. J. Gutmann and J. M. Borrego, “Solar power satellite rectenna design study: directional receiving elements and parallel-series combining analysis,” NASA Final Rep. NAS9-15453, Ch. 3, Dec. 1978.

[19] 三宅 智之, 呉 南健, 雨宮 好仁, “マイクロ波送電に用いる整流素子の最適設計,” Technical report of IEICE, PE-95-8, pp7-12, Jul. 1997.

[20] 谷村 佳則, “5.8GHz 用レクテナの開発,” 学士論文, 京都大学, Feb. 2002.
[21] 山下 榮吉, “マイクロ波シミュレータの基礎,” (社)電子情報通信学会, Mar. 2004.
[22] H. A. Wheeler, “Transmission-line properties of a strip on a dielectric Sheet on a plane,” IEEE Trans. Microwave Theory and Tech., Vol. MTT-25, pp.631-647, 1977.
[23] 小西 良弘, “マイクロ波回路の基礎とその応用,” 総合電子出版社, Aug. 1990.
[24] 谷口 慶治, “マイクロ波電子回路 –設計の基礎-,” 共立出版, Mar. 2004.
[25] 加藤 肇, 見城 尚志, 高橋 久, “図解・わかる電子回路 –基礎から DOS/V 活用まで-,” 講談社, Sept. 1995.
[26] “Free-space microwave power transmission study-combined phase III and final report: Appendix I,” Raytheon Company, NASA-CR-144151, Sept. 1975.
[27] J. O. Mcspadden, T. Yoo and K. Chang, “Theoretical and Experimental Investigation of a Rectenna Element for Microwave Power Transmission,” IEEE Trans. Microwave Theory and Tech., Vol. 40, pp. 2359-2366, Dec. 1992.
[28] J. O. Mcspadden, L. Fan and K. Chang, “Design and Experiments of a High-Conversion-Efficiency 5.8GHz Rectenna,” IEEE Trans. Microwave Theory and Tech., Vol. 46, pp. 2053-2060, Dec. 1998.
[29] 篠原 真毅, 岡田 寛, 三谷 友彦, 松本 紘, “マイクロ波エネルギー伝送用レクテナ整流回路のパラメータ最適化に関する研究,” 第 24 回 宇宙エネルギーシンポジウム講演論文集 pp. 125-129, Mar. 2005.
[30] Yong-Chae Jeong, Jong-Sik Lim, ”A Novel Frequency Doubler Using Feedforward Techique and Defected Ground Structure”, IEEE Microwave and Wireless Components Letters, Vol.14, No.12, Dec.2004
[31] Shif-Chieh Yen, Tah-Hsiung Chu, ”A Retro-Directive Antenna Array With Phase Conjugation Circuit Using Subharmonically Injection-Locked Self-Oscillating Mixers”, IEEE Transactions on Antennas and Propagation, Vol.52, No.1, Jan.2004

学会発表

- 第 26 回 宇宙エネルギーシンポジウム，神奈川, 3 月, 2007.
  “MAV 搭載用マイクロ波エネルギー受電システム”
- 第 27 回 宇宙エネルギーシンポジウム，神奈川, 3 月, 2008.
  “MAV 搭載用マイクロ波エネルギー伝送システム”
- 第 10 回宇宙太陽発電衛星(SPS)シンポジウム，千葉, 8 月, 2007.
  “5.8GHz フェーズドアレイを用いた小型飛行体へのエネルギー伝送”
- 45th AIAA Aerospace Sciences Meeting and Exhibit, Reno, Nevada, Jan. 2007.
  “Power Transmission to a Micro Aerial Vehicle”
- 46th AIAA Aerospace Sciences Meeting and Exhibit, Reno, Nevada, Jan. 2008.
  “A MAV Flight using Microwave Power Supply”

学会誌掲載

- 第 26 回 宇宙エネルギーシンポジウム 講演論文集, 2007.
- 第 27 回 宇宙エネルギーシンポジウム 講演論文集, 2008.
- AIAA paper, 2007.
- AIAA paper, 2008

AWARD

- AIAA paper, 2007
  “AIAA BEST PAPER AWARD, 2007”

東京大学 大学院新領域創成科学研究科
基盤科学研究系
先端エネルギー工学専攻

平成 19 年度

修士論文

Microwave Beam Power Rectification System

― マイクロ波エネルギー伝送高効率受電システムの開発 ―

2008 年 2 月提出
指導教員 小紫 公也 准教授

66210 小松 周平

Chapter 1
Introduction

This chapter shows the background and the issues of this thesis.

1.1 Objective of our research

The objective of this study is “To develop the microwave energy supply system”. We aim to transmit microwave to a flying vehicle for its propulsion system and other tasks. In order to achieve this system, it is necessary to develop high power transmitters and receivers. And it also needs the beam controlling technology and the target acquisition and tracking technology, which we will describe mainly in this study. For the beam control, we considered the method of phase shifting. The phase shift method enables us to control a microwave beam by electrically sending signal not by mechanically rotating antennas and to steer the beam to a flying target quickly. For the target acquisition and tracking, we considered the software retro-directive system and the amplitude comparison method. This system can acquire a flying target by simple analyzing of the pilot signal from the target and does not need so complicated devices.

Our research was originally one part of “Innovative Aerial Robot Project (IARP)”, which is being carried out as part of the 21st century COE program, “Mechanical Systems Innovation”. In this project, the Micro Aerial Vehicle (MAV) or Unmanned Aerial Vehicle (UAV) is designed to execute by itself some missions such as observation and support for emergency rescue. Here we charged the propulsion system and considered to supply energy to the MAV by microwave transmission.

This microwave transmission technology also can be useful for saving an airplane which would lack fuel and be crashing on the ground. Assuming that, in some kind of accident, the airplane would have shortage of fuel and could not avoid emergency landing, the microwave energy supply apparatuses which were placed at some points could refuel the airplane in the air and support the airplane to land on safer places. Like this, the microwave transmission system can become one of very useful methods to save those human lives.

1.2 Problem with MAV circling

There are two main problems with MAV circling: target tracking and output power shortage. Figure1.1 shows moving MAV.

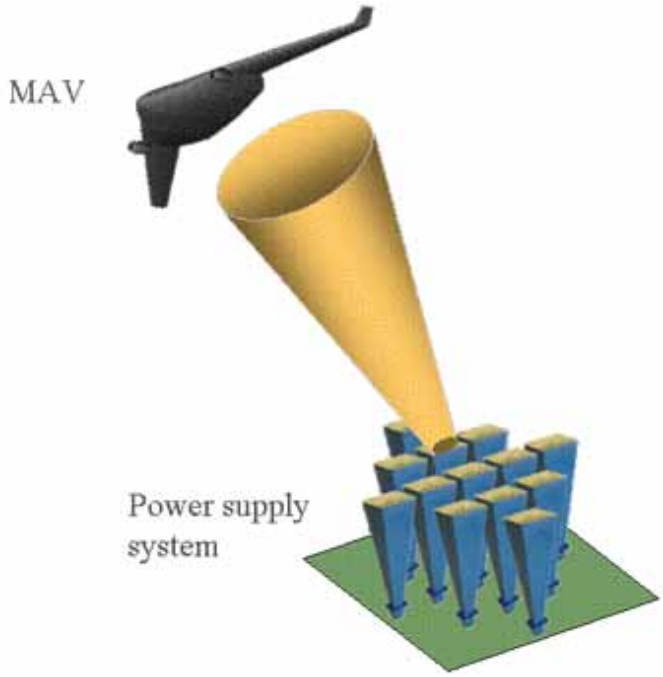

Figure 1.1 Imaginary picture

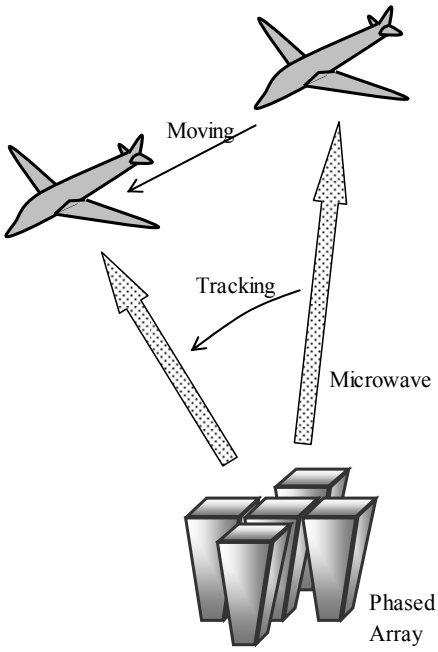

Figure 1.2 Schematic of issues

1.2.1 Target Tracking

The target position changes continuously because the MAV is moving, and then we required the target tracking system. It consisted of the three parts: tracking system, phase controlling and power transmitting. Figure1.3 shows its schematic.

First, MAV transmits the pilot signal to the tracking system. Figure1.4 shows the block diagram of the tracking system. The incident pilot signal is received by two or three antennas, and the microwave elements are divided and combined, and then rectified and measured as the output voltages. From the measured voltages, we can find the incident angles of the pilot signal, or the target position. With this target position, the shifting phases for each transmitting antenna lines are calculated and the instructions of the phase shift are sent to the phase shifters. As seen in Figure1.5 the microwaves with phase controlled reinforce each other to a beam steering angle of θ_{str} expressed as:

$$d \sin \theta_{str} = \frac{\lambda \delta}{2\pi} \tag{1.1}$$

which λ is the wavelength and δ is the phase difference.

Figure1.6 shows the computed and measure beam profiles. Measured main-lobe fractional energy and main-lobe beam divergence angle are well agreed with the calculated ones. Figure1.7 shows the computed properties as a function of θ_{str}. The beam divergence was constant at about nine degrees, which corresponds to the beam quality of M^2=1.6.

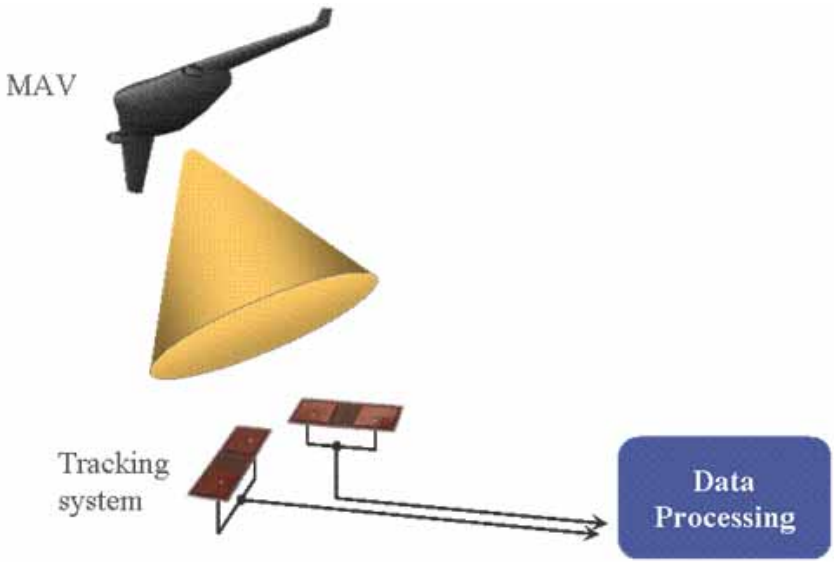

Figure 1.3 Schematic of target tracking system

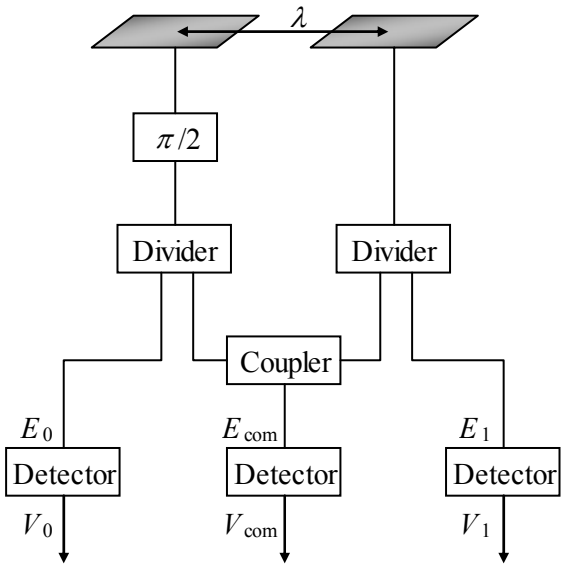

Figure 1.4 Block Diagram of Tracking System

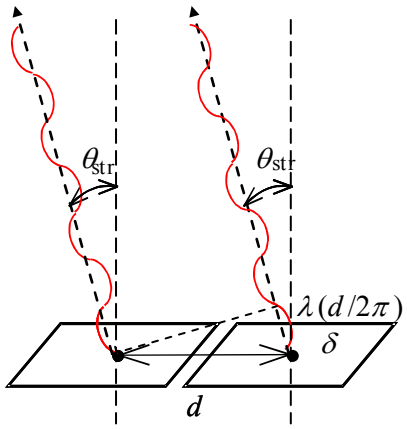

Figure 1.5 Schematic of Beam Steering by Phased Array Antennas

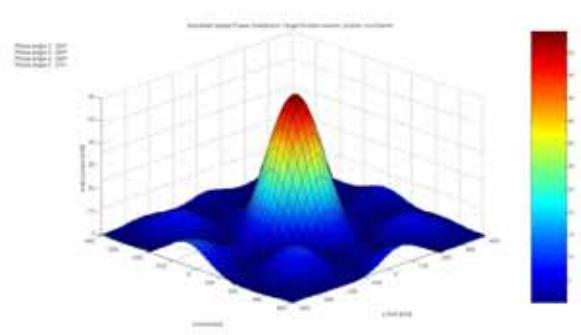

a) Computed

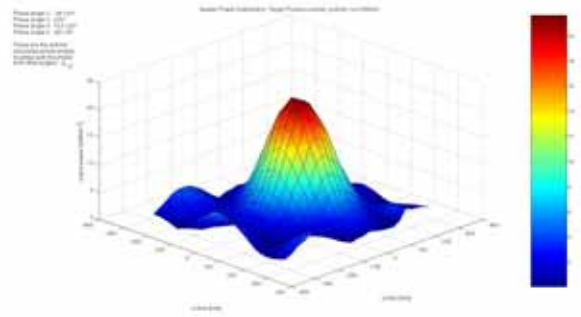

b) Measured

Figure 1.6 E_y Distribution at h=1m

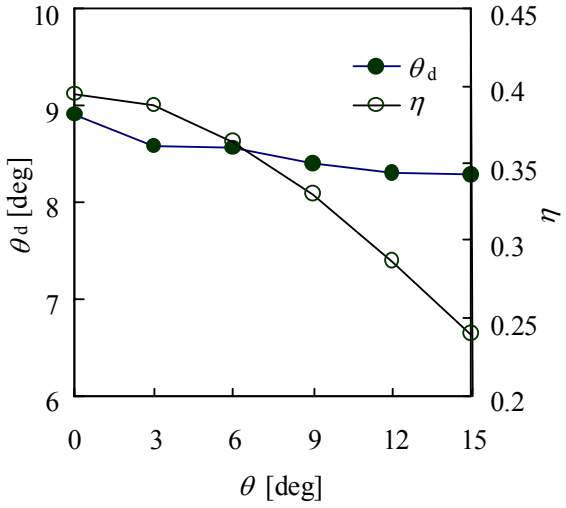

Figure 1.7 Computed Main-lobe Fractional Energy and Beam Divergence Angle

1.2.2 Output Power Shortage

For MAV flying with microwave power supply system, I regarded a lack of output power in this system as the most important problems on present showing. To obtain electric power enough to drive a motor on a MAV, increasing conversion efficiency of rectifier and rectenna should be made an array. The output power in one recntenna is increased more than motor of MAV needed and then, the impedance matching with the load resistance was enabled by making the rectennas parallel. As a result, we can achieve the maximum conversion efficiency, RF-DC. Figure shows the rectennas parallel. I show the more details in the chapter 2.

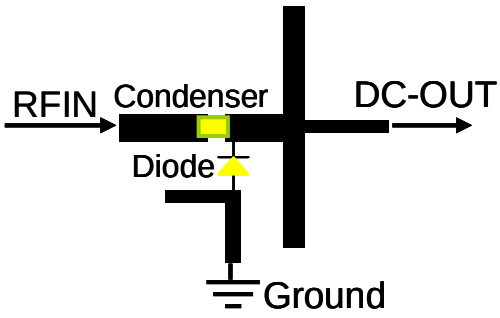

Figure 1.8 Rectifier Circuit

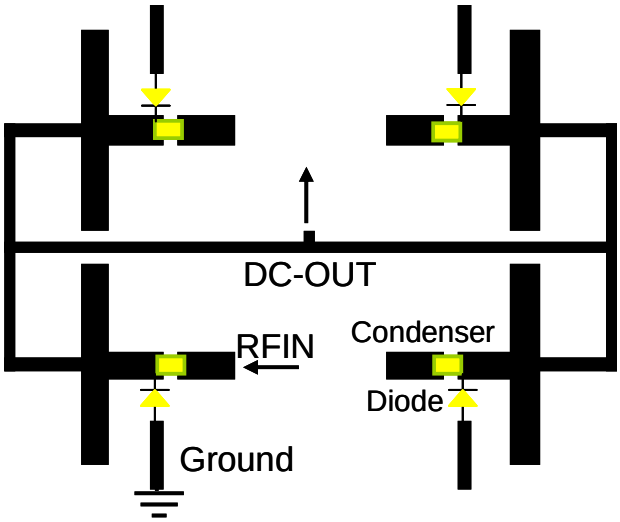

Figure 1.9 Parallel Rectennas Circuit

1.2.3 Other Applications with Power Transmitting System

For IARP, we developed the power transmitting system and the power receiving system with microwave for MAV, and we can apply the technology to wider areas. One of the advantages of this system is supplying power continuously within the microwave receivable area, without installing batteries or connecting to the power supplier by wire. Therefore, the technology will be suitable for such robot as searching for and rescuing victims trapped under heavy debris by disasters and as scanning and discovering and repairing cracks and other troubles of pipes with moving in it.

Moreover, the polarity-free rectenna, developed in my study, especially achieved the stable power supply independent from the incident wave polarization in its small size. I consider that we can apply this technology to micro robots moving independently without remote control and mobile devices running not with batteries but with the receiving power in spaces filled with microwave.

1.3 Objective of this thesis

Our system has these issues which are described. In these problems, most important point that should be solved, it is to obtain electric power enough to drive the electric motor on an MAV which synchronized with the power transmission energy. For that, the objective of my paper is improvement of rectifier and making high efficiency rectennas array.

Chapter 2
Theory of Energy Transmission System

This chapter shows theory of energy transmission system.

2.1 Transmission Horn Antennas Array Design

First, for simplicity, we assume that there are two point wave sources with spacing d, which are coupled in-phase. The electromagnetic fields radiated from one point wave source are:

$$E = E_0 \exp(\kappa r) \tag{2.1}$$

where kappa is the free-space wave number,

$$\kappa = 2\pi/\lambda \,. \tag{2.2}$$

And then the composite electromagnetic fields radiated from these two point wave sources are expressed as:

$$E_{com} = E_1 \exp(i\kappa r_1) + E_2 \exp(i\kappa r_2) \tag{2.3}$$

The condition for maximizing these composite fields amplitude is:

$$\kappa(r_1 - r_2) = 2n\pi \tag{2.4}$$

Assuming that the fields are sufficiently far from the two point wave sources, Eq(2.4). It is approximated with the spacing d and angle alpha with the vertical axis in the following form:

$$\kappa d \sin\alpha = 2n\pi \tag{2.5}$$

or, replacing $\kappa = 2\pi/\lambda$, we can rewrite this equation as follows:

$$d \sin\alpha = n\lambda \tag{2.6}$$

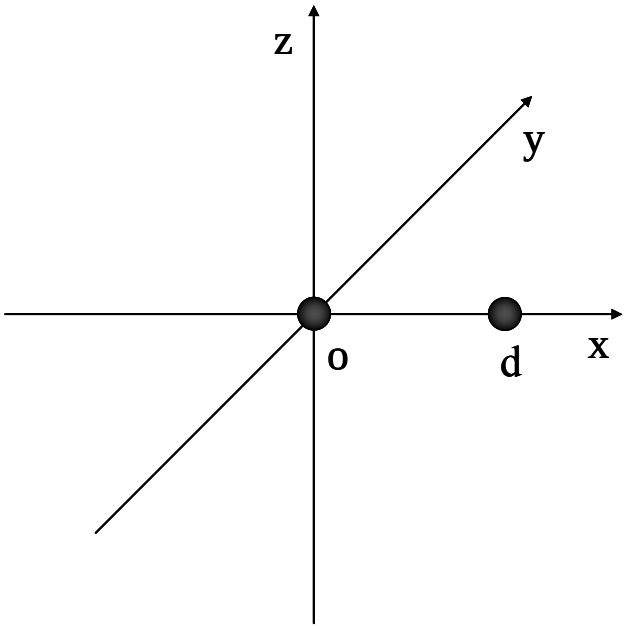

Figure 2.1. Simple model of two wave sources

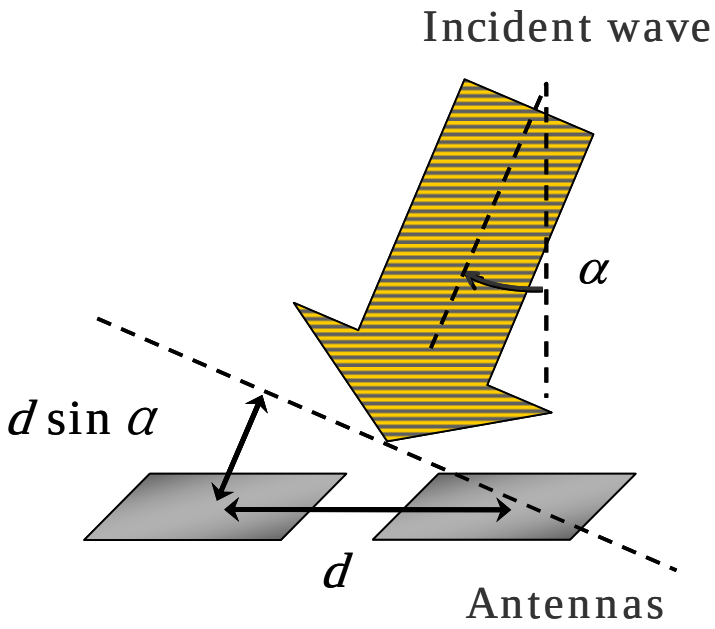

Figure 2.2 Relation of incident wave and phase difference

Now we shift the wave source phase by theta against the other wave source. The amplitude of the composite electromagnetic fields is:

$$E_{com} = E_1 \exp(i\kappa r_1) + E_2 \exp i(\kappa r_2 + \theta) \tag{2.7}$$

The maximizing condition is similar to the case of in-phase coupling:

$$\kappa d \sin\alpha = 2n\pi + \theta \tag{2.8}$$

In order to maximizing the electromagnetic field at an angle alpha with the vertical axis, setting n = 0, the phase to shift is expressed as following form:

$$\theta = \kappa d \sin\alpha \tag{2.9}$$

Taking into account that theta varies from -pi to pi, the Eq. becomes:

$$-\arcsin(\lambda/2d) \le \alpha \le \arcsin(\lambda/2d) \tag{2.10}$$

In this way the steering angle interval can be determined from the wave length lambda and the antenna spacing d.

Let be the electric flux density D, magnetic flux density B, electric field E, magnetic filed H

$$\begin{aligned} div\mathbf{D} &= \rho \qquad & div\mathbf{B} &= 0 \\ rot\mathbf{H} - \frac{\partial \mathbf{D}}{\partial t} &= \mathbf{i} \qquad & rot\mathbf{E} + \frac{\partial \mathbf{B}}{\partial t} &= 0 \end{aligned} \tag{2.11}$$

where, with the permittivity ε, permeability μ and electric conductivity σ, we have the following relation

$$\mathbf{D} = \varepsilon\mathbf{E} \qquad \mathbf{B} = \mu\mathbf{H} \qquad \mathbf{i} = \sigma\mathbf{E} \tag{2.12}$$

With the angular frequency ω, Eq (2.11). can be expressed in the components

$$\begin{aligned} (\nabla^2 + \omega^2\varepsilon\mu - j\omega\mu\sigma)E_i &= 0 \\ (\nabla^2 + \omega^2\varepsilon\mu - j\omega\mu\sigma)H_i &= 0 \qquad i = x, y, z \end{aligned} \tag{2.13}$$

where gamma is the cutoff wavenumber

$$\gamma = \sqrt{\omega^2\varepsilon\mu - j\omega\mu\sigma} \tag{2.14}$$

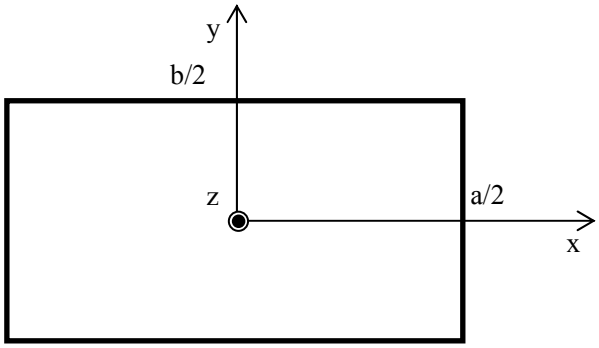

Figure 2.3. Aperture of rectangular waveguide

In rectangular waveguides, the condition and boundary conditions are:

$$\begin{aligned} \sigma &= 0 \\ E_y &= 0 \;\; at \;\; x = \pm a/2 \\ E_x &= 0 \;\; at \;\; y = \pm b/2 \end{aligned} \tag{2.15}$$

Assuming the propagation fields along the guide direction

$$\mathbf{E} = \mathbf{E}(x,y)e^{j\omega t-\beta z}, \qquad \mathbf{H} = \mathbf{H}(x,y)e^{j\omega t-\beta z} \tag{2.16}$$

where beta is the propagation wavenumber along the guiding direction. Then we have the each field component is

$$\begin{aligned} E_x &= -\frac{j\omega\mu}{\beta^2+\omega^2\varepsilon\mu}\frac{n\pi}{b}H_0 \sin\frac{2m\pi}{a}x\cdot\cos\frac{2n\pi}{b}y\cdot e^{j\omega t-\beta z} \\ E_y &= \frac{j\omega\mu}{\beta^2+\omega^2\varepsilon\mu}\frac{m\pi}{a}H_0 \cos\frac{2m\pi}{a}x\cdot\sin\frac{2n\pi}{b}y\cdot e^{j\omega t-\beta z} \\ E_z &= 0 \end{aligned} \tag{2.17}$$

$$\begin{aligned} H_x &= -\frac{\beta}{\beta^2+\omega^2\varepsilon\mu}\frac{2m\pi}{a}H_0 \cos\frac{2m\pi}{a}x\cdot\sin\frac{2n\pi}{b}y\cdot e^{j\omega t-\beta z} \\ H_y &= -\frac{j\omega\mu}{\beta^2+\omega^2\varepsilon\mu}\frac{2n\pi}{b}H_0 \sin\frac{2m\pi}{a}x\cdot\cos\frac{2n\pi}{b}y\cdot e^{j\omega t-\beta z} \\ H_z &= H_0 \sin\frac{2m\pi}{a}x\cdot\sin\frac{2n\pi}{b}y\cdot e^{j\omega t-\beta z} \end{aligned}$$

In this experiment, the parameters are

$$\begin{aligned} f &= 5.8\times10^{9} \ \ ,Hz \\ \omega &= 2\pi f = 3.64\times10^{10} \ \ ,rad/s \\ \varepsilon &= 8.84\times10^{-12} \ \ ,F/m \\ \mu &= 1.26\times10^{-6} \ \ ,H/m \\ a &= 0.04 \ \ ,m \\ b &= 0.02 \ \ ,m \end{aligned} \tag{2.18}$$

So, the number of m, n are decided to

$$m = 1,\ \ n = 0 \tag{2.19}$$

and thus, we obtain the following propagation fields:

$$\begin{aligned} E_x &= 0 \\ E_y &= E_0 \cos\frac{\pi}{a}x \cdot e^{j\omega t-\beta z} \\ E_z &= 0 \\ H_x &= -\frac{\gamma}{j\omega\mu}E_0 \cos\frac{\pi}{a}x \cdot e^{j\omega t-\beta z} \\ H_y &= 0 \\ H_z &= -H_0 \sin\frac{\pi}{a}x \cdot e^{j\omega t-\beta z} \end{aligned} \tag{2.20}$$

This field is found to be constant along the y-direction and have only the y-component. So we do not have to consider the x and z component.

The plane waves in wave guides change to spherical waves in radiating to the free space. So when we consider the radiation fields in the aperture plane, we have to take the path difference into account. Setting the base length to the path length along the z-axis, the path difference is:

$$\delta_{sph} = \frac{\pi l}{\lambda}\left(\left(\frac{x}{l_a}\right)^2 + \left(\frac{y}{l_b}\right)^2\right) \tag{2.21}$$

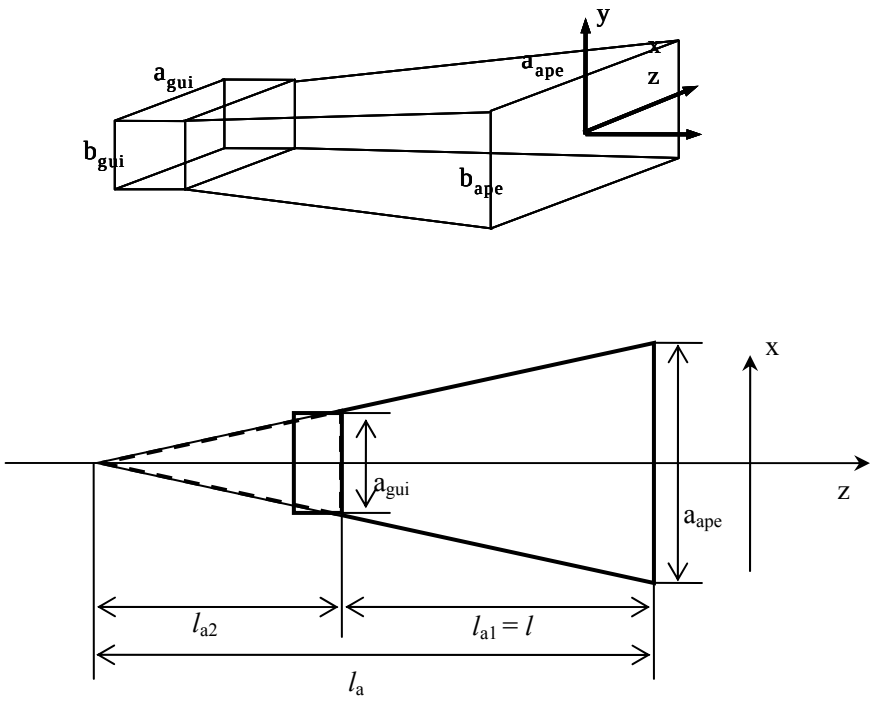

Figure 2.4. Horn antenna

Assuming the electric field at the center in the aperture plane is E_{oy}, the y-component of the electric field is:

$$E_y = E_{0y} \cos\frac{\pi x}{a_2} \exp\left(-j\delta_{sph}\right) \tag{2.22}$$

Next we regard the electromagnetic field propagating toward the positive z-direction as the radiation field from the set of electric and magnetic unit currents. The combined field become:

$$\begin{aligned} E_{\alpha y} &= -\xi \frac{E_y}{4\pi} \frac{j\beta}{r} \left(\cos\alpha_x + \cos\alpha_y\right) e^{-j\beta r} \\ H_{\alpha x} &= E_{\alpha y} / \eta \\ E_r &= E_{\alpha x} = H_r = H_{\alpha y} = 0 \end{aligned} \tag{2.23}$$

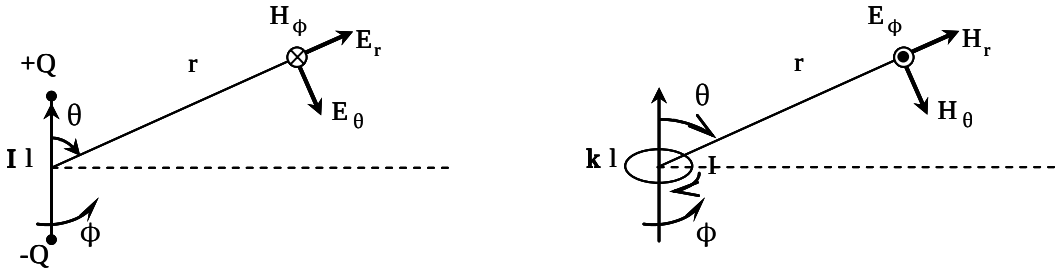

Figure 2.5.Electric and Magnetic unit currents

Thus we can obtain the radiation field from the horn antenna by integrating Eq (2.23). in the aperture plane of the horn antenna:

$$E_{\alpha y} = \xi \frac{j\beta E_{0y}}{4\pi} \frac{e^{-j\beta r}}{r} \left(\cos\alpha_x + \cos\alpha_y\right) \int_{-\frac{a}{2}}^{\frac{a}{2}} dx \int_{-\frac{b}{2}}^{\frac{b}{2}} dy \cos\frac{\pi x}{a_2} \exp\left(-j\delta\right)$$

$$\begin{aligned} H_{\alpha x} &= E_{\alpha y} / \eta \\ E_r &= E_{\alpha x} = H_r = H_{\alpha y} = 0 \end{aligned} \tag{2.24}$$

Figure2.6 shows two patterns of the transmission antenna array, one-dimensional antenna array and two-dimensional antenna array. The one-dimensional antenna array was composed of three horn antennas which arranged in a line along the x-axis. And a two-dimensional antenna array was composed of five horn antennas which arranged crosswise on the x-axis and y-axis. In both cases, the horn antenna spacing d was 120 mm.

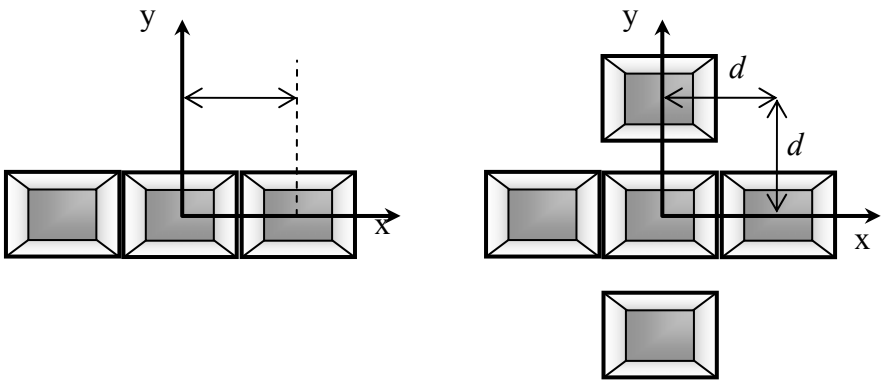

(a) one-dimensional type (b) tow-dimensional type

Figures 2.6. Transmitting antenna array

Although, in some existing experiments, the receiver was fixed at a certain point and the transmitter was rotated in order to measure its directional characteristics, we moved the receiver and did not move the transmitter because of the transmitter complexity and the receiver simplicity.

Figure2.7 represents the block diagram of the transmitter system. This is the case of the one-dimensional antenna array. Firstly we divided microwaves from the 5.8GHz oscillator into three lines. Here we used a four-ways power divider, and so, terminated the forth port and used only the other three ports. And then we shifted each of the microwave phases by the 6-bit digital phase shifters. These phase shifters have insertion losses which change depending on phase-shifting patterns. Thus we amplified the microwaves by two steps. The driver amplifier amplified the power which significantly decreased by the phase shifters' insertion losses. Next the power amplifier amplified to the necessity power level, that is, from several milliwatts to about seven hundred milliwatts. The power amplifiers' output power values are shown in the table2.1.

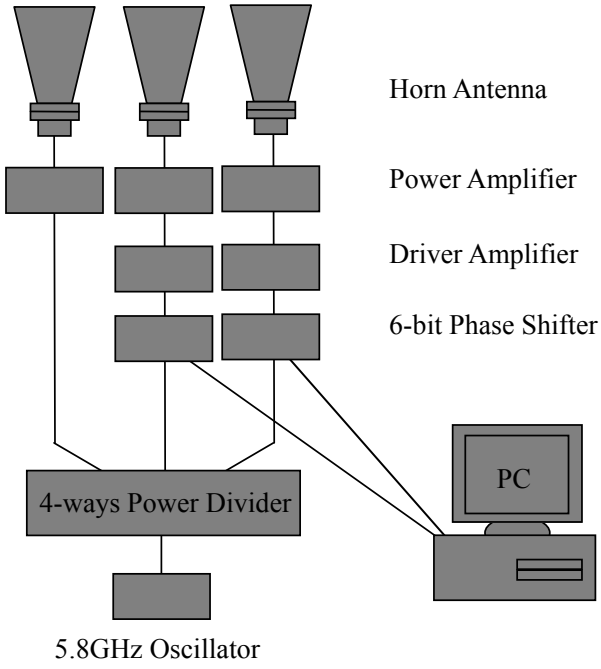

Figure 2.7. Block diagram of the transmission system with three antennas

Figure2.8 shows the block diagram of transmitter system in the case of two-dimensional antenna array. This system used the 8-ways power diver, not the 4-ways power divider. So we terminated the last three ports and used only the first five ports. The power amplifiers' output power values are shown in table.

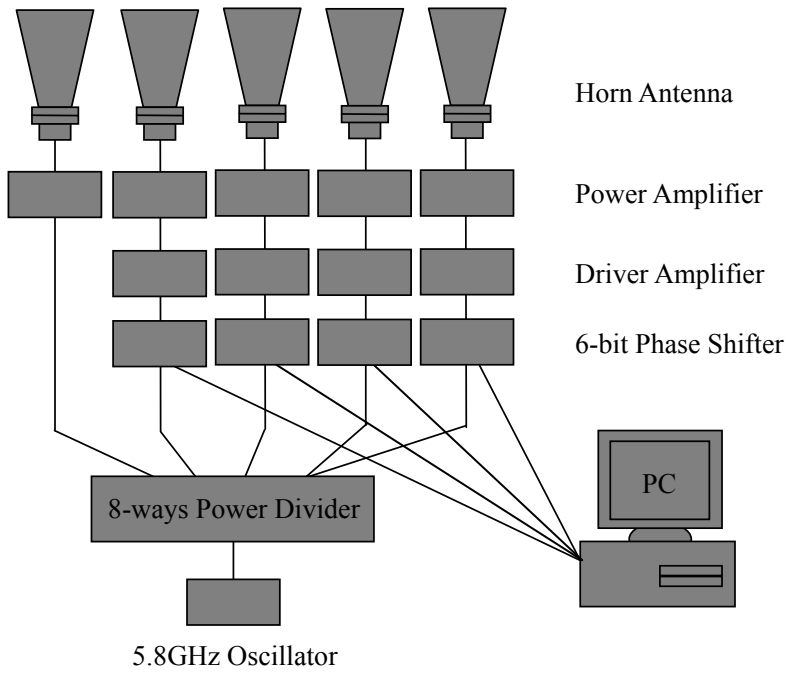

Figure 2.8. Block diagram of the transmission system with five antennas

The phase shifting signals were sent electrically from a computer to each phase shifter. More precisely we input phase shifting patterns by C language cords, and then, according to these phase shifting patterns, a digital output module “PCI2798” sent voltage output patterns to the phase shifters. Each connector assignment is shown in table. Six connectors per phase shifter were assigned, and each of these six connectors had two voltage patterns, that is, on and off. Therefore the number of signal patterns which each digital phase shifter had was $2^6 = 64$. Fig. represents the phase shifting command entry screen. So we controlled digitally each microwave phase.

Table 2.2 Port assignment to each phase shifter

Connector No.	Connector name	Phase shifter	
		Pin No.	No.
3	IN/OUT1	1	2
4	IN/OUT2	2	
5	IN/OUT3	3	
6	IN/OUT4	4	
7	IN/OUT5	5	
8	IN/OUT6	6	
9	IN/OUT7	no connection	
10	IN/OUT8	no connection	
11	IN/OUT9	1	3
12	IN/OUT10	2	
13	IN/OUT11	3	
14	IN/OUT12	4	
15	IN/OUT13	5	
16	IN/OUT14	6	
17	IN/OUT15	no connection	
18	IN/OUT16	no connection	
31	IN/OUT17	1	4
32	IN/OUT18	2	
33	IN/OUT19	3	
34	IN/OUT20	4	
35	IN/OUT21	5	
36	IN/OUT22	6	
37	IN/OUT23	no connection	
38	IN/OUT24	no connection	
39	IN/OUT25	1	5
40	IN/OUT26	2	
41	IN/OUT27	3	
42	IN/OUT28	4	
43	IN/OUT29	5	
44	IN/OUT30	6	
45	IN/OUT31	no connection	
46	IN/OUT32	no connection	
51	IN/OUT33	1	extra
52	IN/OUT34	2	
53	IN/OUT35	3	
54	IN/OUT36	4	
55	IN/OUT37	5	
56	IN/OUT38	6	
57	IN/OUT39	no connection	
58	IN/OUT40	no connection	

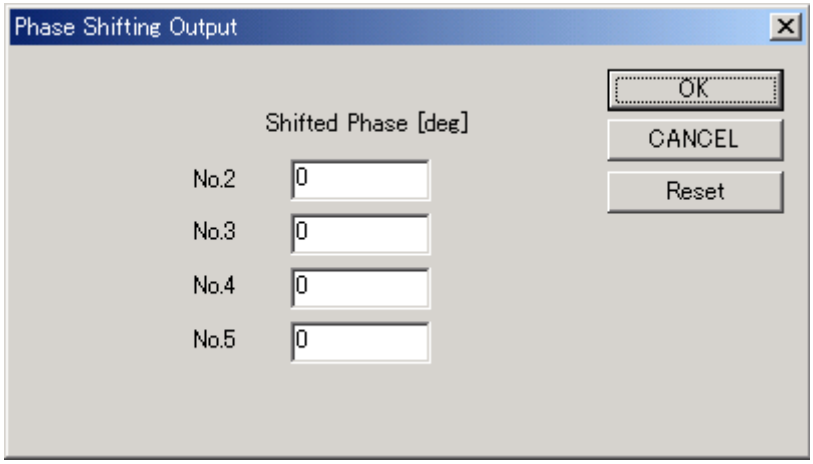

Figure 2.9. Phase shifting signal input form

2.2 Characteristics of a horn antenna

Figure2.10. shows the radiation field levels at 530 mm high from one horn antenna. The radiated power was rectified to DC by the detector “PE8016” in open circuit, so the output in the vertical axis is represented in the unit of millivolt. Theoretically the radiation field level from one horn antenna is symmetric. Thus the filed levels are expected to be the same at 150 mm and -150 mm in y-direction and similarly the same at 150 mm and -150 mm in x-direction. Figs. and show the better symmetry in the y-direction than the x-direction.

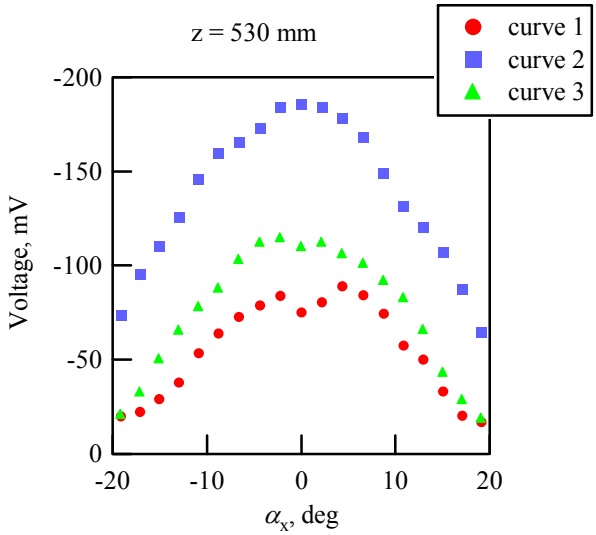

(a) Radiation field at 530 mm high, measured along the x-axis

Curve1: alpha_y = -15.8 deg, Curve2: alpha_y = 0 deg, Curve3: alpha_y = 15.8 deg

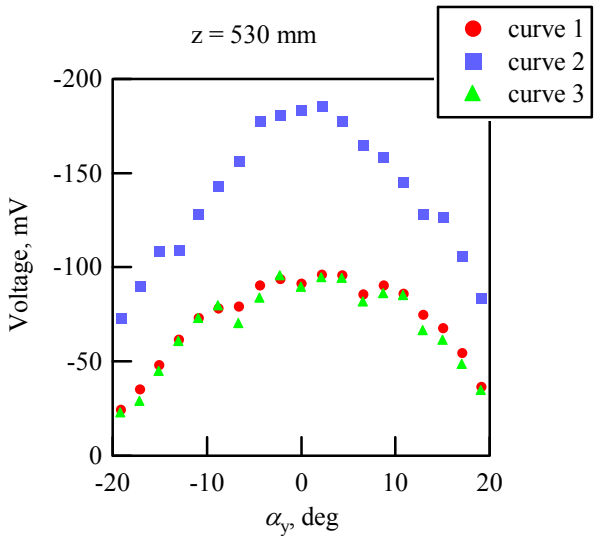

(b) Radiation field at 530 mm high, measured along the y-axis

Curve1: alpha_x = -15.8 deg, Curve2: alpha_x = 0 deg, Curve3: alpha_x = 15.8 deg

Figures 2.10. Measured radiation field from one horn antenna in the xy-plane

The relation of field levels and distances from the transmitter are shown in Figures2.11 and in each of the xz-plane and yz-plane. From these graphs we can see that the microwaves were radiated from the transmitter aperture plane and expanded to the free space.

The radiated power level decreases as the height becomes greater. Figure2.12 shows the relation of the heights from the transmitter and the measured voltages along the z-axis, which compares with the calculated results. The calculated value was inversely proportional to the square distance. On the other hand the measured value was inversely proportional to the distance to the power of about 1.7.

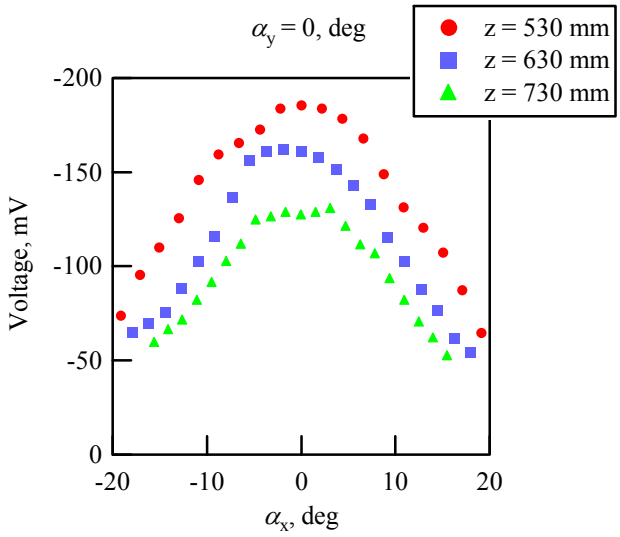

(a) Radiation field at alpha_y = 0 deg, measured along the x-axis

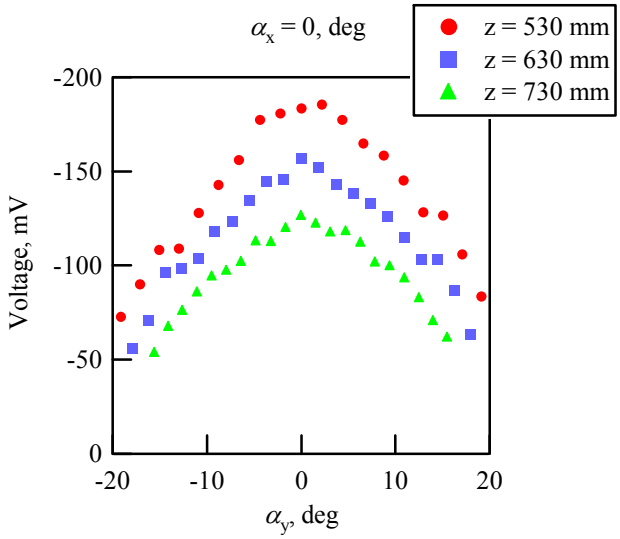

(b) Radiation field at alpha_x = 0 deg, measured along the y-axis

Figures 2.11. Measured radiation fields from one horn antenna with the parameter of height

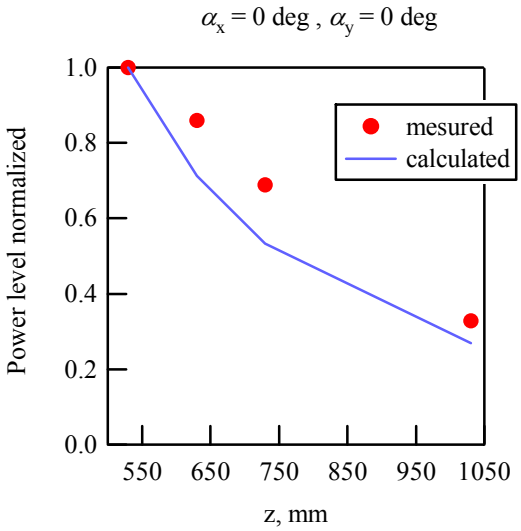

Figure 2.12. Comparison of measured and calculated field from one horn antenna with the parameter of the height

Figure2.13 shows the 3-dB width in the xz-plane and yz-plane, which is the full width. It can be said that the measured data was good agreement with the calculated data and constant with the height. Additionally the 3-dB width seems to be the same in the both of the xz-plane and yz-plane although the aperture rectangle has the long side in the x-direction and the short side in the y-direction.

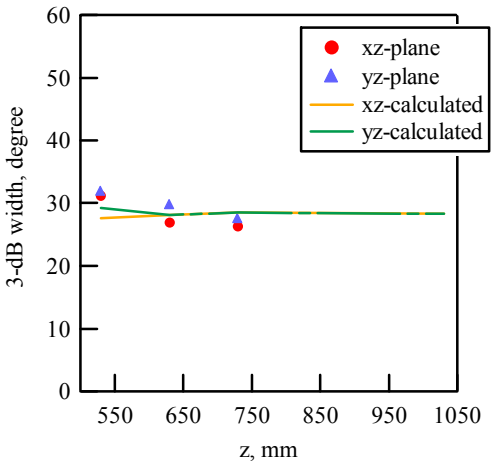

Figure 2.13. Comparison of measured and calculated 3-dB width

2.3 Characteristics of a one-dimensional array

As you shift the each microwave phase against the central antenna's one, you can turn the microwave beam to a certain range of direction as shown in Figures2.14. The range is determined from the antenna spacing d relative to the wave length lambda. In the case of this experimental one-dimensional array, the range was from deg to deg.

As the beam turned to the side, the maximum voltage in main lobes decreased whereas the maximum voltage in side lobes increased, which were called grating lobes. Fig shows the calculated results in the same phase shifting condition with the experiments. If the microwave beam gets at the angle of deg with the vertical axis, there appeared two equal-power lobes as expected from Figs.

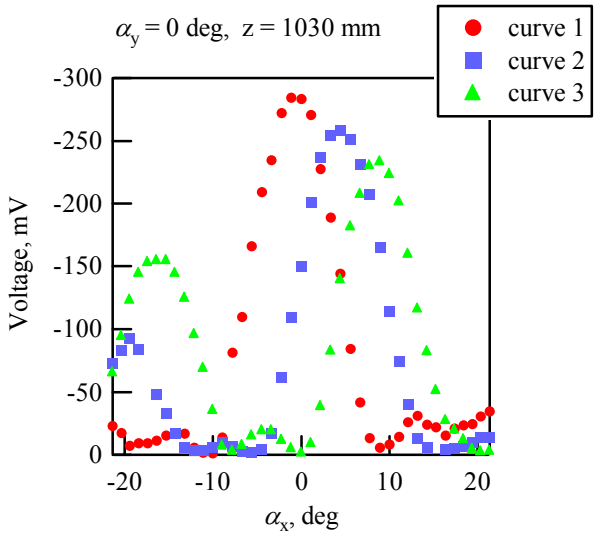

(a) Measured data. Each phase-shift is as follows

Curve1: deg, Curve2: deg, Curve3: deg

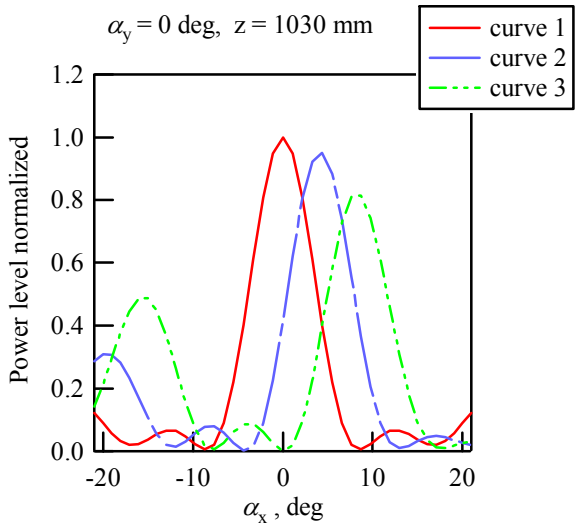

(b) Calculated data. Each phase-shift is as follows

Curve1: deg, Curve2: deg, Curve3: deg

Figures 2.14. Radiation fields from one-dimensional antenna array with the phase-shift control

The measured results were in good agreement with calculated results as shown in Figure2.15 The 3-dB widths of main lobe were 10.6 deg in measured data and 7.7 deg in calculated data.

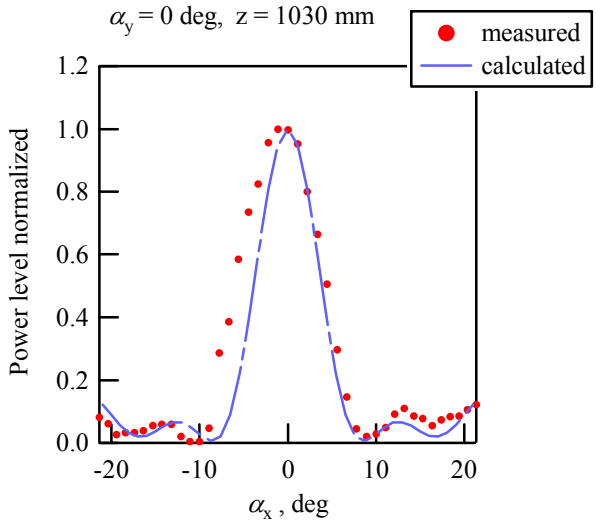

Figure 2.15. Comparison of measured and calculated radiation field from one-dimensional antenna array at 1030 mm high

2.4 Characteristics of a two-dimensional array

In the case of two-dimensional arrays, similarly, we can turn the microwave beam by shifting the each microwave phase. Figures2.16. show the controlled microwave beams in measured data and calculated data. These curves had also main lobes and some side lobes. The characteristics seemed to be the same as those of one-dimensional arrays.

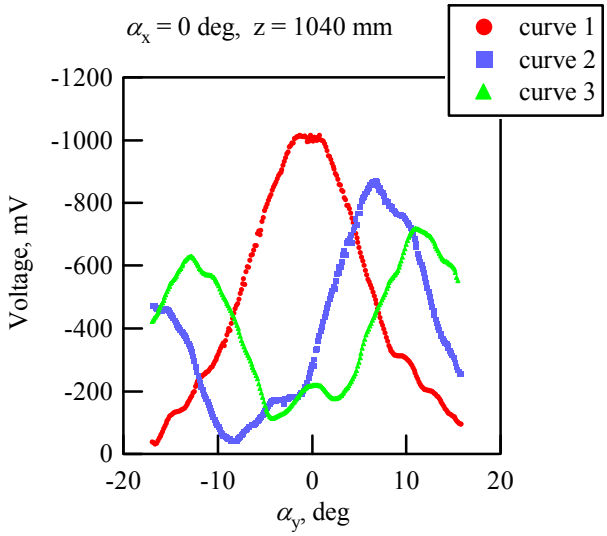

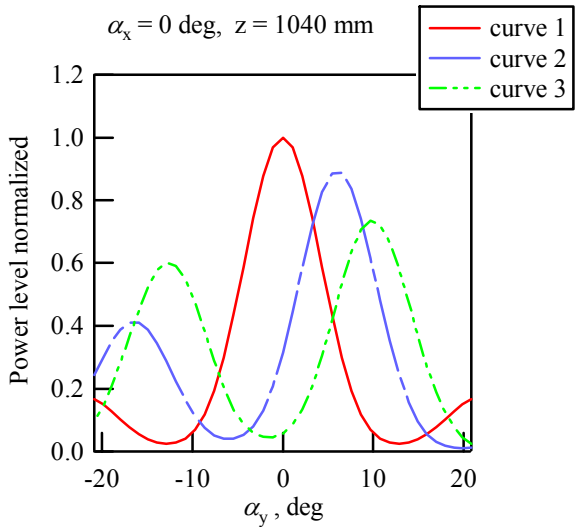

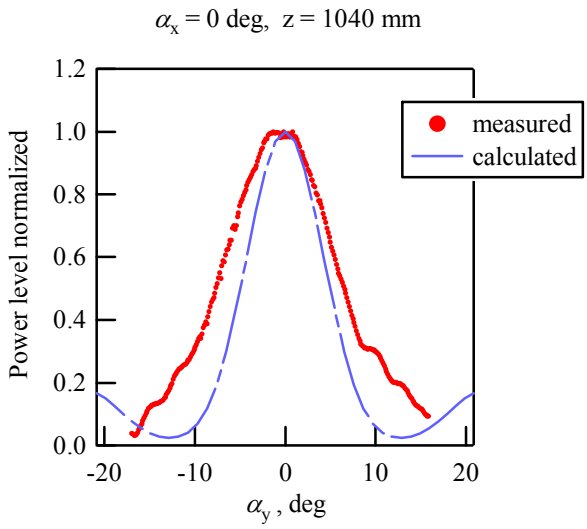

Figures 2.16. Comparison of measured and calculated radiation field from two-dimensional antenna array at 1040 mm high

The 3-dB widths of main lobes were 14.2 deg in measured data and 9.8 deg in calculated data, which seem to be slightly greater than those of one-dimensional arrays. However, considering in the xy-plane, the main lobes obviously became narrower in the two-dimensional array as Figures2.17 show.

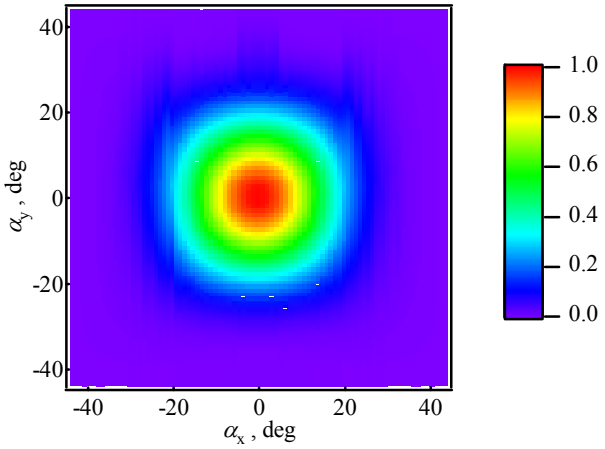

(a) Radiation field from one horn antenna

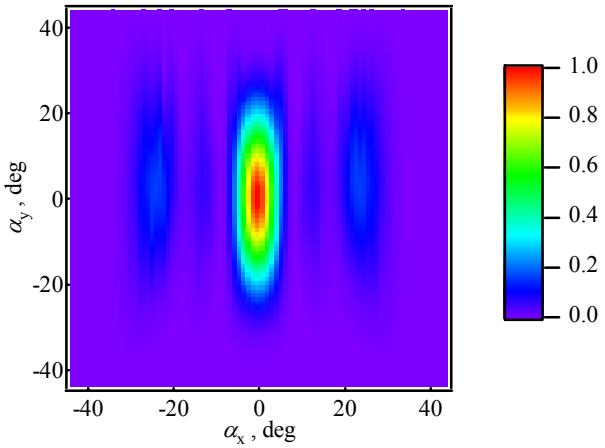

(b) Radiation field from one-dimensional horn antenna array

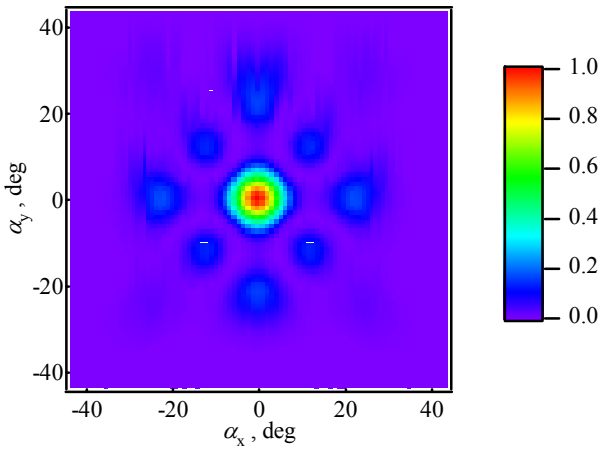

(c) Radiation field from two-dimensional horn antenna array

Figures 2.17. Simulated radiation fields from three types of antenna arrays at 1040 mm high. The plot is represented in the xy-plane. Figure 2.18 shows Beam diameter depends on distance from horn antenna.

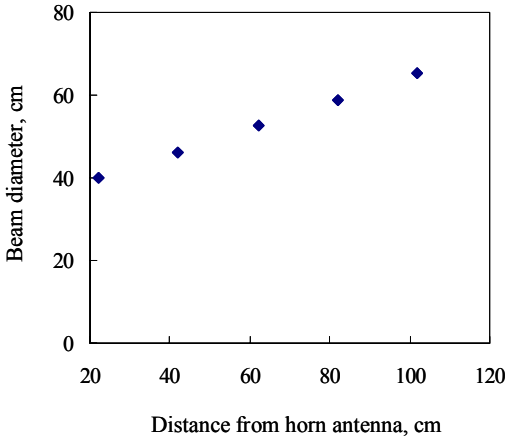

Figure 2.18 Beam diameter

Chapter 3
Theory of Energy Receiving System

This chapter shows theory of receiving system including antenna elements and rectifier circuit elements.

3.1 Theory of Rectenna Design

"Rectenna" is a device receiving the transmitted microwave power as radio frequency (RF) and converting alternating current (AC) to direct current (DC) by rectifying. It is the coined term for "RECTifier" and "antENNA". Figure3.1 shows its schematic. It normally consists of a receiving antenna, an input filter, a rectifier and a output filter for smoothing power. Since the receivable power with a rectenna is not enough large to operate systems, we use as a array of some rectennas arranged and connected in series and in parallel each other.

One of the determining factors of the power conversion efficiency of a rectenna is the characteristic of the important element of a rectifier, or a diode. Figure3.2 shows the RF-DC conversion efficiency characteristic of a rectenna. When the input power P_{in} decrease, the conversion efficiency η will become reduced. It is because the voltage between the both ends of a diode V_d will become smaller than the diode forwarding voltage V_f, and then the rectifying feature of the diode will not work (the V_f effect). Although the conversion efficiency increase as P_{in} becomes larger, when V_d surpass the diode breakdown voltage V_R, η will also become reduced. It is because the reverse current starts to flow (the V_R effect). Moreover, η will also become reduced because the high order radio-frequency re-radiation generated with rectifying (the higher order harmonics effect).

Furthermore, the load resistance connected to the rectenna output has the optimal values; it is the value in matching the output impedances of the rectenna with the load and also depends on P_{in}., Although there is no reflected wave with connecting the optimal load, there is reflected waves and η decreased without it. As a result, the diode maximum efficiency curve has a peak value depending on the input power P_{in} and the load resistance R_L.

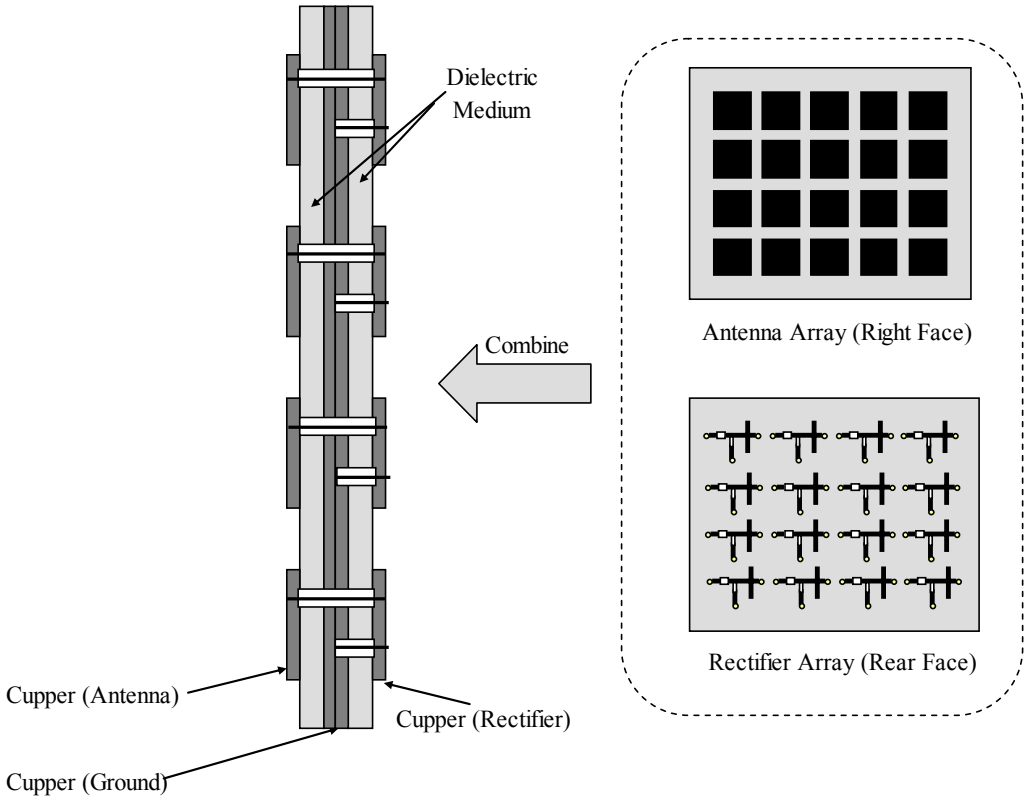

Figure 3.1 Schematic of Rectenna

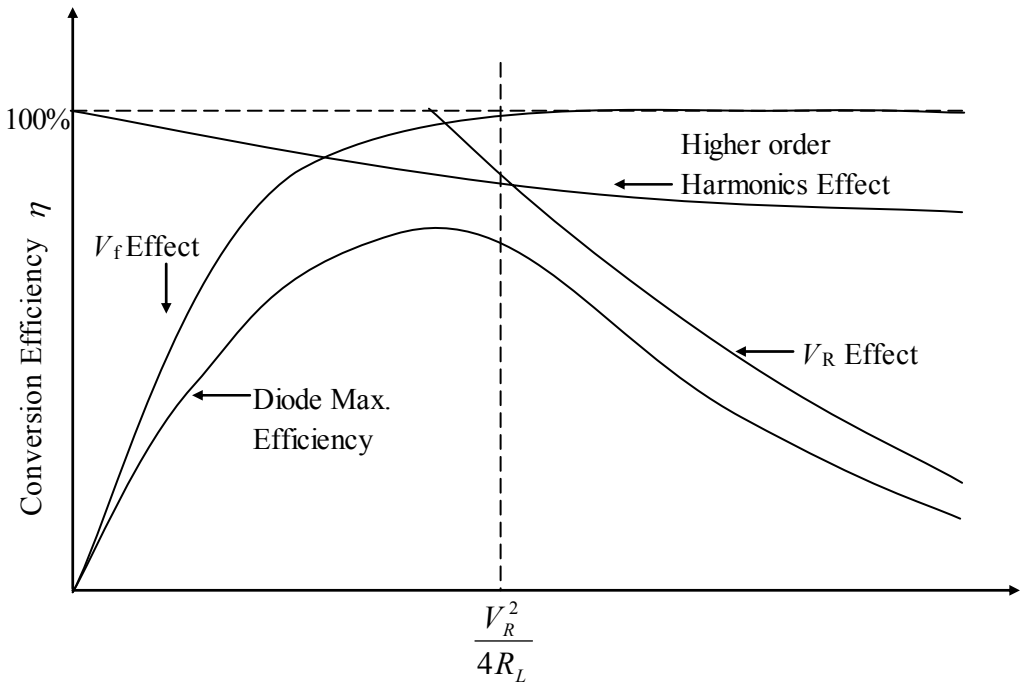

Figure 3.2 RF-DC Conversion Efficiency of Rectenn

3.2 Theory of Antenna Design

There are many kinds of Antenna; horn antennas, monopole antenna, dipole antennas, slot antennas, *etc*. In this thesis, we adopted the plane patch antennas because of the simplicity of structure, the miniaturization in the size and the lightness.

The typical examples of the plane antennas are MSA (Micro Strip Antenna) elements. They function as the microwave radiators composed of the planar circuit resonance elements with the circular or quadrangular open boundary on the printed circuit boards (PCBs). Generally the substrate for the MSA require low dielectric constant (ε_r = 1.2~5.0) and low dielectric loss ($\tan\delta$=10^{-3}~10^{-4}), such as the teflon-fiberglass substrate. In request for weight saving of wider band width (low Q value), the paper-honeycomb substrate are used.

The size of the MSA elements is normally the half wavelength or less. The main mode is used as a specimen excitation mode, and the MSA radiation pattern of the main mode shows the unidirectionality with the maximum value in the front direction (z-axis) of the antenna pattern of both the circular and quadrangular MSA. Thus, MSA enables to achieve the unidirectional pattern without additional reflectors and to compose the thin and compact antenna simply.

3.2.1 Size Designing of MSA

The size of antennas depends on the target microwave wavelength. Generally the half wavelength resonance method is used, and its resonance direction length is $\lambda_g/2$. The λ_g is the wavelength of the microwave passing through a medium and is approximately expressed by:

$$\lambda_g = \frac{\lambda_0}{\sqrt{\varepsilon_r}} \tag{3.1}$$

where λ_0 is the free-space wavelength and ε_r is the dielectric constant of the medium. In this thesis, the size of square MSA for 5.8GHz was about 1.22cm on a side, 1.484cm^2 with the glass-epoxy substrate FR-4 (ε_r=4.7). I explain the more details in 3.2.3

3.2.2 Impedance Matching Method between MSA element and Feeding System

Figure3.2 shows the typical feeding methods of the MSA. The input impedance Z_{in} of the MSA excited in the main mode depends on the predetermined feeding point ρ_0. Z_{in} at the resonance point and around the near frequency domain vary from 0 (center) to several hundred ohms (open boundary) by ρ_0. Thus, with feeding at the edge (open boundary) of the MSA elements, the resonance Z_{in} exhibits a high impedance characteristic about 300~500Ω. Consequently, we need for it to match up with the feeding system about 50Ω of the characteristic impedance. In the backside-coaxial feeding method, we can match up the impedances by offsetting the position ρ_0 of the feeding point F. Generally, the offset ratio is about 30%; (ρ_0/a)=0.3 in the circular MSA,

($\rho_0/(a/2)=0.3$) in the quadrangular MSA. In the coplanar feeding method, we can also match up the impedance of the antenna with one of the main feeding line F_m by the $\lambda_g/4$ impedance transformer T_f. In the electromagnetic coupling feeding method, it is adopted to set the insert length l_0 to the specimen excitation slot of the feeding strip line at about $\lambda_g/4$, and to control the values of the specimen excitation slot width w, its slot length l_s and the offset length ρ_0. In this thesis, we adopted the backside-coaxial feeding method and 0.3 of ρ_0 because of the simplicity of its fabrication and the connectivity with the rectifier circuits.

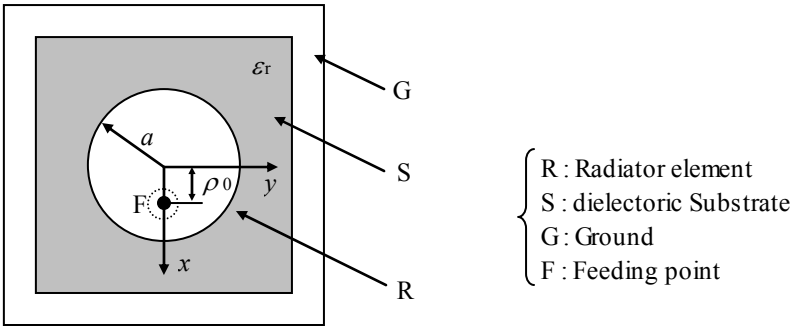

a) Backside-Coaxial Feeding Method

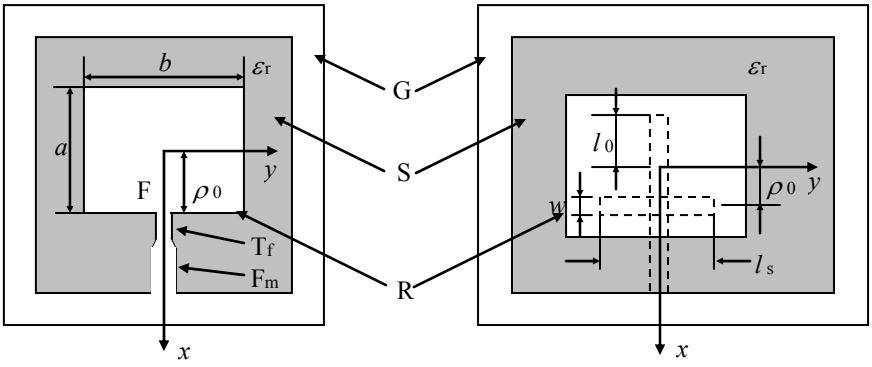

b) Coplanar Feeding Method c) ElectroMagnetic (EM) Coupling Feeding Method

Figure 3.3 Feeding Methods of MSA Element

3.2.3 Interior Electromagnetic Field of Rectangular MSA

Figure3.3 shows the analysis model of the inner electromagnetic field of a rectangular MSA. When the substrate thickness t is enough smaller than the free-space wavelength λ_0 ($k_0 t << 1$; k_0 is a free-space wavenumber), TM_{mn0} wave is excited; it has an electric field element only to the direction of t (z direction).

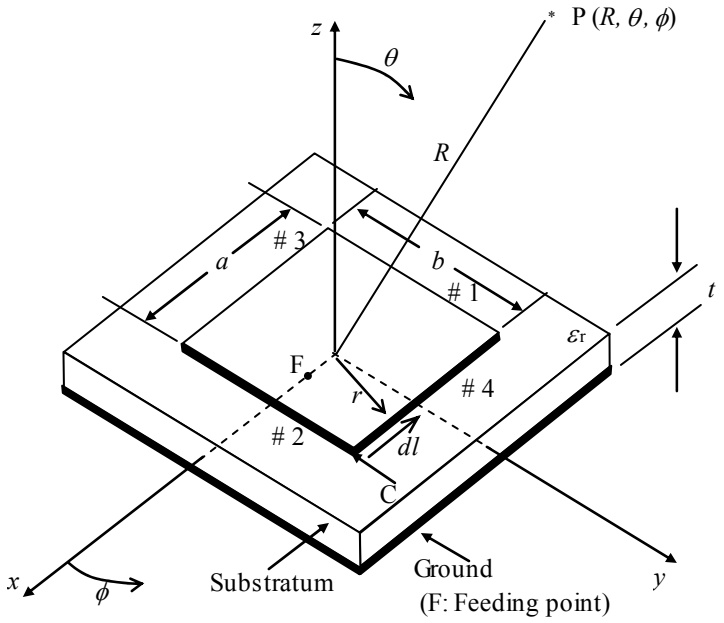

a) Coordinate System

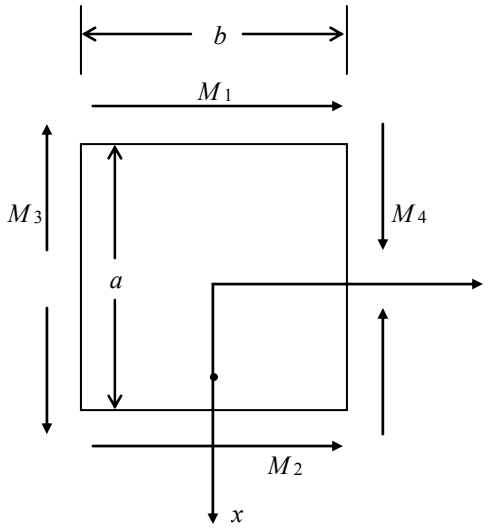

b) Example of Magnetic Current

Figure 3.4 Rectanglar MSA and its Coordinate System

The electromagnetic field of this TM_{mn0} wave is expressed by follow wave equation:

$$\left(\nabla^2{}_t + k^2\right)E_z = 0 \qquad \text{(Interior region)} \tag{3.2}$$

$$\frac{\partial E_z}{\partial n} = 0 \qquad \text{(Open boundary)} \tag{3.3}$$

where $\hat{\boldsymbol{n}}$ is outward unit normal vector at the open boundary and $\nabla^2{}_t$ is $\left(\partial^2/\partial x^2 + \partial^2/\partial y^2\right)$.

When we separate variables of E_z element as $E_z=X(x)Y(y)$ and of k element as $k^2=k_x{}^2+k_y{}^2$ into x and y directions, and assign it to the equation (3.2):

$$\frac{1}{X}\frac{\partial^2 X}{\partial x^2} = -k_x^2 \tag{3.4}$$

$$\frac{1}{Y}\frac{\partial^2 Y}{\partial y^2} = -k_y^2 \tag{3.5}$$

where $k_x=m\pi/a$ of a wavenumber in x direction and $k_y=n\pi/b$ in y direction. by using the separation of variables, E_z element of TM_{mn0} wave is expressed by:

$$E_z = E_0 \cos\left(\frac{m\pi}{a}x + \frac{m\pi}{2}\right)\cos\left(\frac{n\pi}{b}y + \frac{n\pi}{2}\right) \tag{3.6}$$

$$k^2 = \left(k_x^2 + k_y^2\right) = \left[\left(\frac{m\pi}{a}\right)^2 + \left(\frac{n\pi}{b}\right)^2\right] \tag{3.7}$$

where E_0 is an arbitrary number, $k = \omega\sqrt{\varepsilon\mu}$ is the wave number in the dielectric, and m and n are arbitrary integers. Additionally, we assign this E_z to the Maxwell equation and consider the TM wave condition (H_z=0), then we can find the interior electromagnetic elements of the rectangular MSA as:

$$\left.\begin{aligned}
E_z &= \frac{V_0}{t}\cos\left(\frac{m\pi}{a}x + \frac{m\pi}{2}\right)\cos\left(\frac{n\pi}{b}x + \frac{n\pi}{2}\right) \\
H_x &= -\frac{j\omega\varepsilon}{k^2}\cdot\frac{n\pi}{b}\cdot\frac{V_0}{t}\cos\left(\frac{m\pi}{a}x + \frac{m\pi}{2}\right)\sin\left(\frac{n\pi}{b}x + \frac{n\pi}{2}\right) \\
H_y &= \frac{j\omega\varepsilon}{k^2}\cdot\frac{m\pi}{a}\cdot\frac{V_0}{t}\cos\left(\frac{m\pi}{a}x + \frac{m\pi}{2}\right)\cos\left(\frac{n\pi}{b}x + \frac{n\pi}{2}\right) \\
E_x &= E_y = H_z = 0
\end{aligned}\right\} \tag{3.8}$$

where $V_0=tE_0$ is the peak voltage at the edge of the MSA element as a magnetic wall.

In the normal application of the rectangular MSA, TM_{100} or TM_{010} wave as the lowest order mode (basic mode) is important. The interior electromagnetic field of This TM_{100} wave can be find by the equation (3.8) as:

$$\left.\begin{aligned} E_z &= -\frac{V_0}{t}\sin\left(\frac{\pi}{a}x\right) \\ H_y &= \frac{j\omega\varepsilon}{k^2}\cdot\frac{\pi}{a}\cdot\frac{V_0}{t}\cos\left(\frac{\pi}{a}x\right) \\ E_x &= E_y = H_x = H_z = 0 \end{aligned}\right\} \tag{3.9}$$

and Figre3.4 shows the schematic of its electromagnetic distribution considering the edge effect.

Furthermore we can find the resonance frequency f_r of TM_{100} wave with assigning m=1, n=0 and $k = \omega\sqrt{\varepsilon\mu}$ as:

$$f_r = \frac{v_0}{2a\sqrt{\varepsilon_r}} \tag{3.10}$$

where υ_0 is the light speed, ε_r is the dielectric constant of the specimen substratum. When we calculate the resonance frequency of the rectangular MSA, we need to consider the fringing effect:

$$f_r = \frac{v_0}{2a_{eff}\sqrt{\varepsilon_r}} \tag{3.11}$$

where a_{eff} is the equivalent side length and ε_e is the effective dielectric constant, and they are expressed as:

$$\left.\begin{aligned} a_{reff} &= a\left\{1+0.824\frac{t}{a}\cdot\frac{(\varepsilon_e+0.3)[(a/t)+0.262]}{(\varepsilon_e-0.258)[(a/t)+0.813]}\right\} \\ \varepsilon_e &= \frac{\varepsilon_r+1}{2}+\frac{\varepsilon_r-1}{2}\left(1+10\frac{t}{a}\right)^{-0.5} \end{aligned}\right\} \tag{3.12}$$

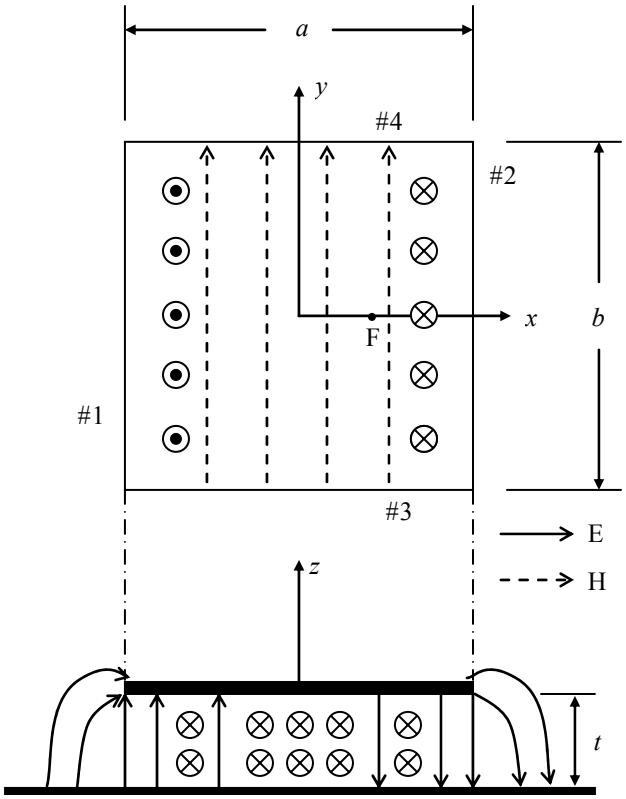

Figure 3.5 Schematic of Electromagnetic Distribution of TM_{100} wave

3.3 Theory of Recteifier Circuit Design

In order to develop the power conversion efficiency of a rectifier, we need its accurate output equivalent circuit model. There are two independent approaches. Firstly, an approximate closed-form circuit was developed assuming an ideal diode and lossless circuit elements. The output equivalent circuit was obtained analytically. Secondly, a more precise computer-simulation model was used, and the load resistance and plotting the resultant output load line. In other researches, numerous rectifier circuits are possible, and a single shunt model diode rectifier circuit has proven most useful in the development work. Figre3.5 shows an idealized equivalent circuit of this rectifier. The input filter should prevent any of the direct current (DC) and harmonic to flow back through the antenna resistance R_S, but allow current flow at the fundamental radio frequency (RF) ω. The output filter should not only prevent alternating current (AC) components to appear across the load terminals but also allow harmonic currents to flow. In particular, the even harmonics should be allowed to flow since they have the property of having a zero average on each half cycle (harmonics are in phase with respect to fundamental). Therefore, the output filter should allow the even harmonics to flow without any voltage drop, prevent current flow at any of the odd harmonics, and allow DC current flow.

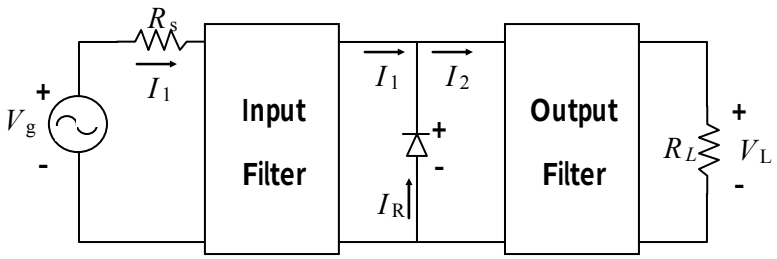

Figure 3.6 Simple Schematic of Rectifier Circuit with Input and Output Filters

3.3.1 Rectifier Circuit Model in Lumped Parameter System

There are two possible implementations of realizing filters with the above characteristics. Figure3.7 shows a method with using lumped circuit elements and satisfying these requirements. The elements L_3, C_3, L_5, C_5, form parallel resonant circuits. They are open circuited at the odd harmonics 3ω, 5ω, respectively. The capacitor C_1 is used for preventing DC flow as well as for series resonating L_3, C_3, L_5, C_5, ... , at the fundamental frequency ω. The L_2, C_2, L_4, C_4, ... , elements in the output circuit are series resonant at the even harmonics 2ω, 4ω, … , respectively. The inductance L_o is assumed to be large enough such that the current I_L is mainly DC. In that way the current I_L would consist of a DC plus even harmonics only.

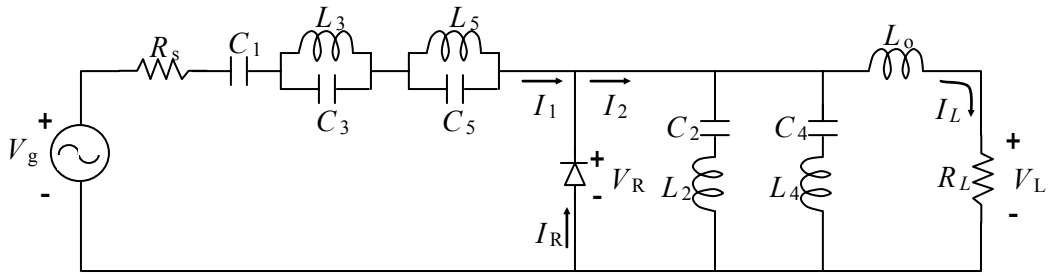

Figure 3.7 Schematic of Rectifier Circuit with Lumped-element Input and Output Filters

Figure3.7 shows another possible method. In this circuit, the output filter consists of a non-dispersive transmission line terminated in a capacitor C_o in parallel with the load R_L; it is a quarter wavelength long at the fundamental frequency. When C_o is enough large, the line can be considered to be at the load end and will appear at the diode terminals as an open circuit at ω,3ω, 5ω, … and as a short circuit at 2ω, 4ω, … ,. Since their rectifier circuit analyses are ideal, we adopted the latter circuit design method in this thesis because of its simplicity. Additionally, I used only the capacitance C_1 as the input filter for simplifying and miniaturizing the circuit patterns. Figure3.8 shows the rectifier circuit pattern and Figure3.9 is its schematic. It consisted only of a chip condenser, a diode and micro-strip lines printed on the substratum.

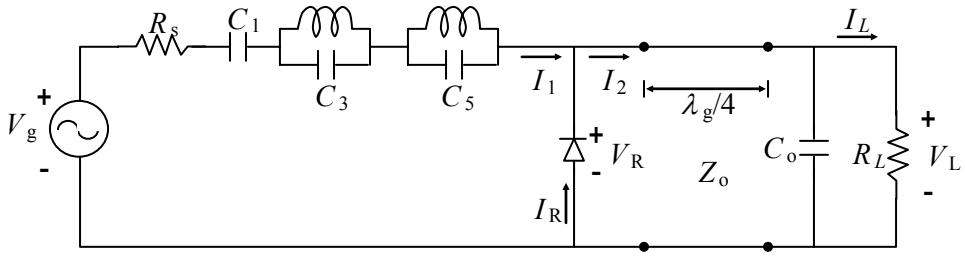

Figure 3.8 Schematic of Rectifier Circuit with a Transmission Line as Output Filter

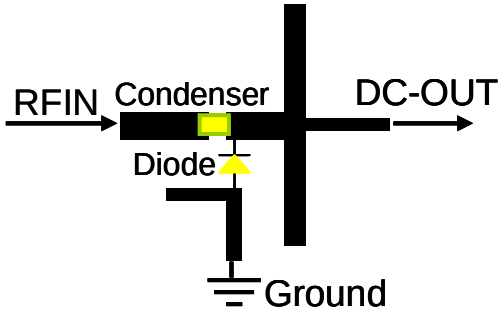

Figure 3.9 Rectifier Circuit Pattern

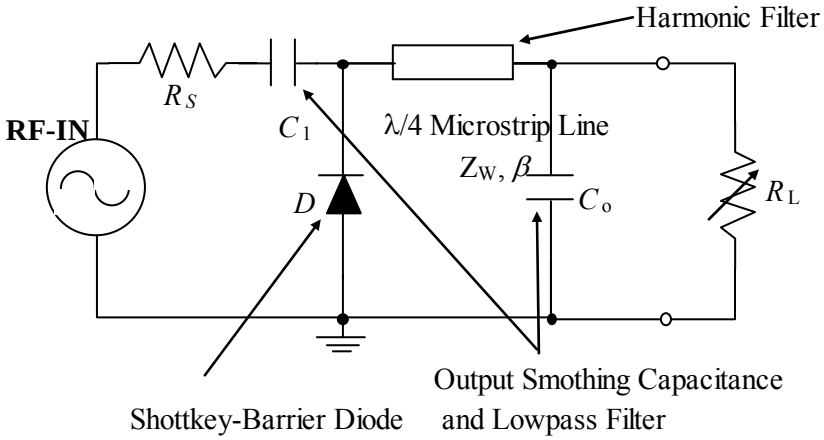

Figure 3.10 Schematic of Rectifier Circuit for Experiment

3.3.2 Matching of Input Impedance

The input line of the rectifier circuit was made as the micro-strip line. The line width W determines the characteristic impedance Z_W of the micro-strip line. Therefore, W is found by Z_W and is expressed as:

$$W = W_0 - \Delta W \tag{3.13}$$

$$W_0 = \frac{8h\sqrt{\left\{\exp\frac{Z_w\sqrt{\varepsilon_r+1}}{42.4}-1\right\}\frac{7+\frac{4}{\varepsilon_r}}{11}+\frac{1+\frac{1}{\varepsilon_r}}{0.81}}}{\exp\frac{Z_w\sqrt{\varepsilon_r+1}}{42.4}-1} \tag{3.14}$$

$$\Delta W = \frac{t}{\pi}\ln\frac{4e}{\sqrt{\left(\frac{t}{h}\right)^2+\frac{1}{\pi^2\left(\frac{W_0}{t}-0.26\right)^2}}} \tag{3.15}$$

where h is the thickness of the dielectric substrate, t is that of the conductor on the substrate, ε_r is the dielectric constant, W_0 is the equivalent width as t=0, and ΔW is the offset of it.

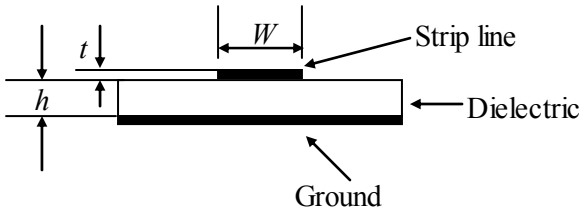

Figure 3.11 Structure of Micro-Strip Line

3.3.3 Design of Stub

In high-frequency circuit, a micro-strip stub with its length $l_S<\lambda_g/4$ plays a role of a capacitor connected in parallel to the circuit. Figure3.11 shows the stub pattern and its equivalent circuit. Its capacitance C_{eq} is expressed as:

$$C_{eq} = \left(\frac{1}{Z_C v'_p} - \frac{1}{Z_0 v_p} \right) l_S \tag{3.16}$$

where Z_0 is the impedance of the transmitting line, Z_C is that of the stub, v_p is the phase speed on the transmitting line and v'_p is that on the stub. The phase speeds are also expressed as:

$$\begin{aligned} v_p &= f\lambda_g = \frac{c}{\sqrt{\varepsilon_W}} \\ &= \frac{c}{\sqrt{\frac{\varepsilon_r + 1}{2} + \frac{\varepsilon_r - 1}{2\sqrt{1+10h/W}}}} \end{aligned} \tag{3.17}$$

$$\begin{aligned} v'_p &= f\lambda'_g = \frac{c}{\sqrt{\varepsilon'_W}} \\ &= \frac{c}{\sqrt{\frac{\varepsilon_r + 1}{2} + \frac{\varepsilon_r - 1}{2\sqrt{1+10h/W_s}}}} \end{aligned} \tag{3.18}$$

where ε_w and ε_w are the effective dielectric constants.

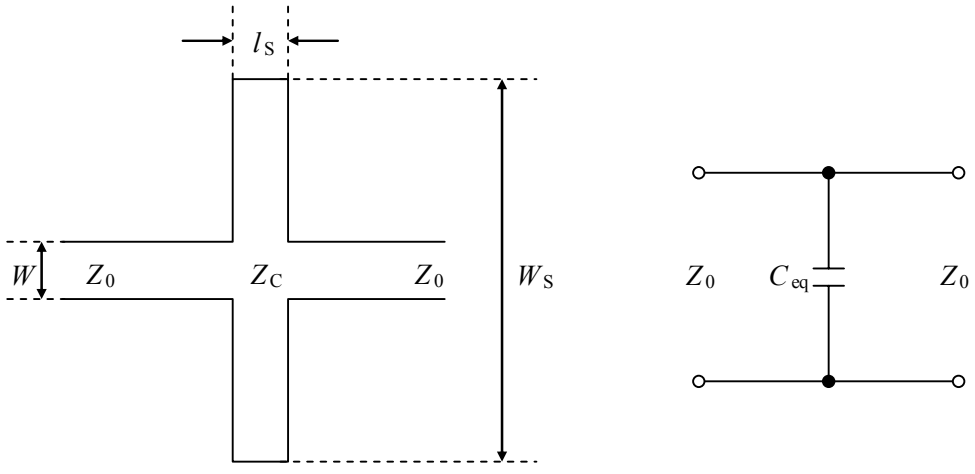

a) Pattern of Micro-Strip Stub b) Equivalent Circuit of Micro-Strip Stub

Figure 3.12 Pattern and Equivalent Circuit of Micro-Strip Stub

3.3.4 Output Load-line Characteristics

Generally the input power P_a is expressed as:

$$P_a = \frac{1}{8}\frac{|V_g|^2}{Z_0}\frac{|1-\Gamma_g|^2}{|1-\Gamma_g\Gamma_0 e^{-j2\beta l}|^2}\left(1-|\Gamma_0 e^{-j2\beta l}|^2\right) \tag{3.19}$$

where Γ_0 is the reflection coefficient of the load and Γ_g is that of the power source. Especially when their impedances matched each other, Γ_0=0 and Γ_g=0, and then;

$$P_a = \frac{1}{8}\frac{V_g^2}{Z_0} \tag{3.20}$$

Since the circuit matched at Z_0=50Ω, the voltage amplitude V_g of the power source with 10mW of the output power is:

$$V_g = \sqrt{8Z_0P_a} = 2(V) \tag{3.21}$$

The rectifier circuit analysis is presented below. Since the current $I_1(t)$ is only of the fundamental frequency and $I_1(t)$ consists only of even harmonics, it follows that:

$$V_L = \frac{\pi}{4}V_g - \frac{\pi^2}{8}R_S I_L \tag{3.22}$$

Figure3.12 shows the characteristic of this equation and indicates follows; from the DC load terminals, the rectifier behave as a DC voltage source of amplitude $(\pi/4)V_S$ and internal resistance $(\pi^2/8)R_S$.

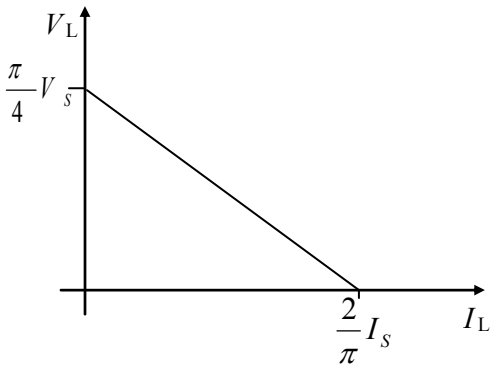

Figure 3.13 Relationship between DC equivalent circuit and load-line

Note that the voltage source is power-level dependent, but the equivalent output resistance is independent of RF power. Using this model, the optimum load for maximum DC load is:

$$(R_L)_{op} = \frac{\pi^2}{8} R_S \tag{3.23}$$

and the maxmum dc power output is:

$$(P_L)_{\max} = \frac{\left(\frac{\pi}{8} V_S\right)^2}{\frac{\pi^2}{8} R_S} = \frac{V_S^2}{8R_S} \tag{3.24}$$

which gives a 100 percent rectification efficiency.

This ideal efficiency has been achieved because it is assumed no losses in any of the circuit components or in the diode. However, since these losses can be minimized by choosing a rectifier diode with small forward drop and small-series resistance and high-Q circuit elements, the closed-form conversion circuit model would be a good approximation to the characteristics of a high efficiency rectenna element.

Additional factors to be considered are the diode nonlinear depletion layer capacitance and package elements. Figure3.13 shows the nonlinear V-I characteristic of a diode; the forward current rises steeply over the forward voltage V_f, and the reverse current increases rapidly over the breakdown voltage V_R.

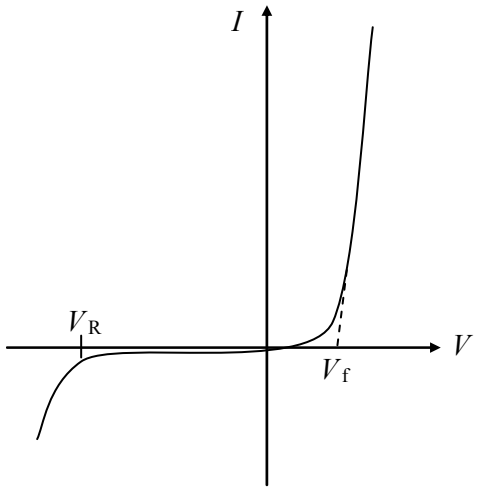

Figure 3.14 V-I Characteristic of Diode

3.3.5 Rectifier Circuit Model in Distributed Parameter System

In order to evaluate the effect of these additional factors, we need a detailed computer simulation model, or distributed parameter circuit model. Figure3.14 shows the equivalent circuit of a diode in the distributed parameter system. With these equivalent circuits, we could express that rectifier circuit pattern (Figure3.8) in the distributed parameter system. Figure3.15 shows the detailed computer simulation model of the rectifier circuit in the distributed parameter system. Although its characteristic was able to be analyzed with general circuit programs, such as SPICE, I could not. It is because the parameters of the diode and the micro-strip lines were not able to be identified; in the high-frequency circuit, the elements induce the capacitances, the reactances and the resistances ,and the parameters of diode vary from production lot to production lot, or from element to element. Therefore, I optimized the rectifier circuit pattern from a pre-designed circuit by changing their parameters independently.

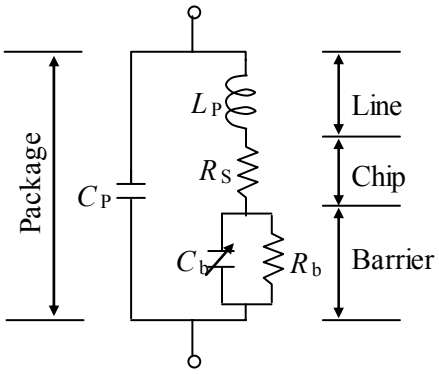

Figure 3.15 Equivalent Circuit of Diode

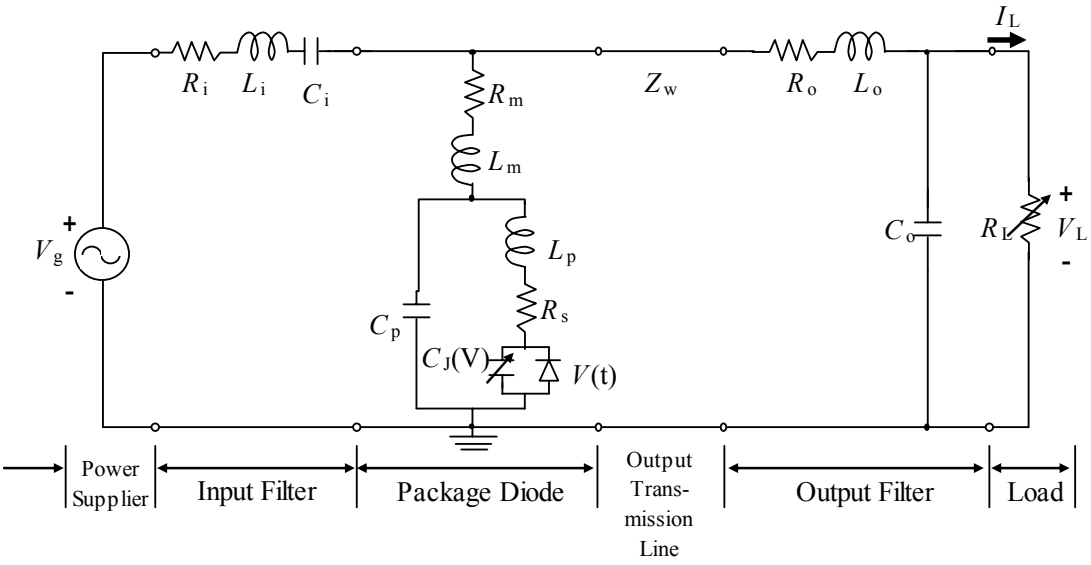

Figure 3.16 Detailed Schematic of Rectifier Circuit for Experiment

3.4 Theory of Polarity-Free Antenna

This describes about the theory of the wave polarization and the methods of making the receiving system polarity-free.

3.4.1 Polarization

There are two polarized waves; linear polarized wave and circular polarized wave. I explain the polarization theories and the reasons why the polarity-free antennas are needed below.

Electromagnetic wave, including microwave, has a polarization. When an electromagnetic wave propagates through an uniform medium, the Maxwell equations are expressed with a charge density ρ=0 as:

$$\left.\begin{aligned} \nabla \times \boldsymbol{E} &= -\mu \frac{\partial \boldsymbol{H}}{\partial t} \\ \nabla \times \boldsymbol{H} &= \sigma \boldsymbol{E} + \varepsilon \frac{\partial \boldsymbol{E}}{\partial t} \\ \nabla \cdot \boldsymbol{E} &= 0 \\ \nabla \cdot \boldsymbol{H} &= 0 \end{aligned}\right\} \tag{3.25}$$

where ε is a dielectric constant and μ is a conductivity of the medium. Generally, an electromagnetic wave varies at a constant frequency as sine curve, the electric field $\boldsymbol{E}$ and the magnetic field $\boldsymbol{H}$ are expressed as:

$$\boldsymbol{E} = \boldsymbol{E}_0 e^{i\omega t} \tag{3.26}$$

$$\boldsymbol{H} = \boldsymbol{H}_0 e^{i\omega t} \tag{3.27}$$

where w is an angular frequency. Since they include phase terms, these $\boldsymbol{E}$, $\boldsymbol{E}_0$, $\boldsymbol{H}$, $\boldsymbol{H}_0$ are complex variables and the absolute values of $\boldsymbol{E}_0$, $\boldsymbol{H}_0$ are the amplitude of the electric field and that of the magnetic field. The real waves are expressed by their real parts.

Moreover, let the partial differentiation about time t $\partial/\partial t = j\omega$ and divide the electrical field and the magnetic field to x, y and z element, then the equation (3.25) is converted as:

$$\left.\begin{aligned}
&\frac{\partial E_z}{\partial y}-\frac{\partial E_y}{\partial z}=-j\omega\mu H_x\\
&\frac{\partial E_x}{\partial z}-\frac{\partial E_z}{\partial x}=-j\omega\mu H_y\\
&\frac{\partial E_y}{\partial x}-\frac{\partial E_x}{\partial y}=-j\omega\mu H_z\\
&\frac{\partial H_z}{\partial y}-\frac{\partial H_y}{\partial z}=(\sigma+j\omega\varepsilon)E_x\\
&\frac{\partial H_x}{\partial z}-\frac{\partial H_z}{\partial x}=(\sigma+j\omega\varepsilon)E_y\\
&\frac{\partial H_y}{\partial x}-\frac{\partial H_x}{\partial y}=(\sigma+j\omega\varepsilon)E_z
\end{aligned}\right\} \tag{3.28}$$

When an electromagnetic wave propagates as a planar wave, there is no change of the electric field and the magnetic field in the *x*-*y* plane at right angles to the propagating direction (*z* axis). Or the solutions differentiating these fields with respect to *x* and *y* are 0. Under this condition, the *z* axial component of the electromagnetic field varying temporally is expressed as:

$$E_z = H_z = 0 \tag{3.29}$$

Figure3.17 shows the electromagnetic wave called "transverse electro magnetic (TEM) wave" or "linear polarized wave;" the temporally homogeneous electromagnetic wave without the component in the propagation direction of the electric field and the magnetic field. Additionally the plane formed by the direction of the electric field and the wave propagating direction is called the "polarization plane."

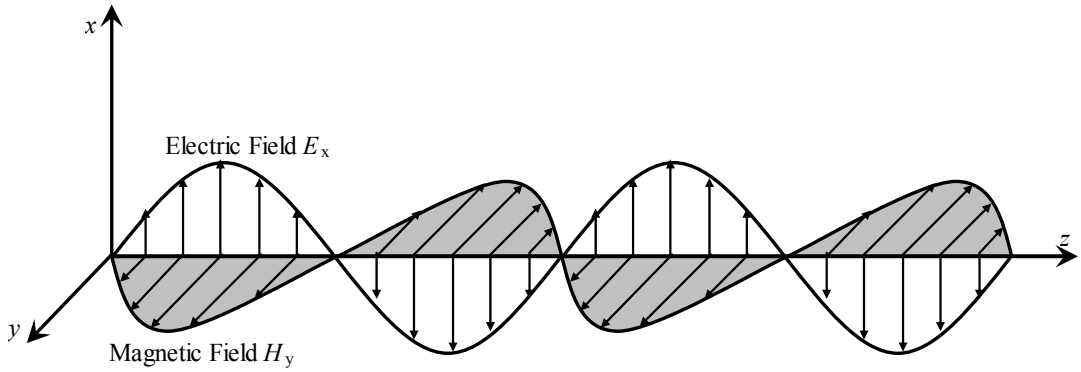

Figure 3.17 Schematic of Planar wave (TEM) Propagation

As a result, the equation (3.29) is figured as:

[*x*-direction polarization]

$$\frac{\partial E_x}{\partial z} = -j\omega\mu H_y$$
$$\frac{\partial H_y}{\partial z} = -(\sigma + j\omega\varepsilon)E_x \tag{3.30}$$

[*y*-direction polarization]

$$\frac{\partial E_y}{\partial z} = -j\omega\mu H_x$$
$$\frac{\partial H_x}{\partial z} = -(\sigma + j\omega\varepsilon)E_y \tag{3.31}$$

The *x*-direction polarization has only an *x* component of the electric field and a *y* component of the magnetic field as Figure3.17, and the *y*-direction polarization is the equivalent of the *x*-direction one rotated by 90 degrees around the propagation direction. Furthermore, they can exist independently of each other. With the linear polarized wave, we can obtain power only with the antennas of the same polarization as the incident wave: the set of horizontal antennas and horizontal wave, or of vertical antennas and vertical wave.

3.4.2 Circular Polarized Wave

Linear polarized waves are able to generate only artificially, and the polarization plane of natural electromagnetic waves are temporally rotating. Figure3.18 shows its schematic. It is called "circular polarized wave." We can generate circular polarized waves by combining the linear polarized waves.

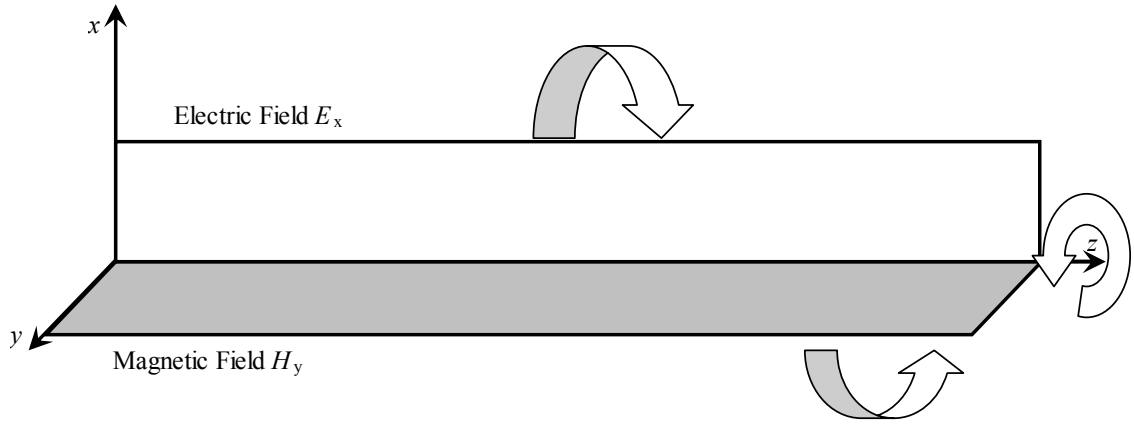

Figure 3.18 Schematic of Rotating Polarization Plane

When there are two linear polarized waves, the electric field component of the *x*-direction polarized wave is expressed as:

$$E_x = a\cos(\omega t - \beta z) \tag{3.32}$$

where β is a phase constant, and that of the y-direction polarized wave with the phase delaying by δ is also expressed as:

$$E_y = b\cos(\omega t - \beta z - \delta) \tag{3.33}$$

When two polarized waves with different phases exist, the circular polarized wave is generated with combining them. (When there is no phase difference, or δ=0, the combined wave is just a linear polarized wave at an angle with the x-axis.)

Under the special condition where $\delta=\pi/2$, $a=b$, E_x and E_y are represented as:

$$\left.\begin{aligned} E_x &= a\cos(\omega t - \beta z) \\ E_y &= a\cos(\omega t - \beta z - \pi/2) = a\sin(\omega t - \beta z) \end{aligned}\right\} \tag{3.34}$$

and then:

$$E_x^2 + E_y^2 = a^2 \tag{3.35}$$

From this, the combined electric field plane is rotating around any z position within its radius a. In turn, this wave is propagating to the z direction at the phase velocity v_p with rotating around the z-axis at the angular rate ω. This wave called "circular polarized wave." Under the general condition where not both $\delta=\pi/2$ and $a=b$, the field locus is the ellipse and the wave called "elliptical polarized wave."

3.4.3 Polarization Choice for MAV

In this thesis, since the objective was the power transmission, not signal transmission, I needed the high-efficient and simple system. The circular polarized wave can ignore the characteristic of the polarization plane. However, it is unsuitable for the power transmission because of its lower transmitting efficiency by reflections with transmitting and receiving than the linear one. The linear one can achieve high efficiency and simple control system, then as with many researches, I adopted it for the power transmitting system. Furthermore, since the MAV will move with random yaw angle in spite of the fixed polarization plane by the linear polarized transmitting wave, we need to make the receiving device polarity-free.

3.5 Methods for Polarity-free

Generally, there are two methods to make receiving antennas polarity-free: one method is a unit of multiple antennas (UMA) with different polarization angles, and another is a self polarity-free antenna (SPFA).

3.5.1 UMA Method

The UMA method is making an antenna-unit combining some normal polarized antennas, such as dipole antennas and patch antennas, and arranging them in predetermined design. It enables to supply stable power as the unit by antenna elements covering for each other's weak angles. Figure3.19 shows the unit of multiple dipole antennas (UMDA). One of the advantages is the calculation simplicity of the polarization-angle dependency and the power conversion efficiency because the UMA consists of the existing antennas. Furthermore, a flexible UMDA sheet has been developed. However, the disadvantages are the low conversion efficiency and the large size because it needs some antennas for achieving polarity-free and the utilizable power is the average obtained from them. Moreover, some rectifier circuits are also needed.

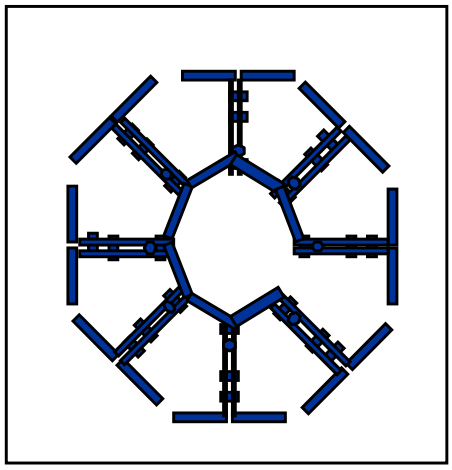

Figure 3.19 Pattern of Unit of Multiple Dipole Antenna

3.5.2 PFA Method

The SPFA method is making an antenna itself polarity-free without any excessive antenna area. The advantage is the smallness of its minimum unit area; about one ninth the size of the UMDA. Moreover, since it requires only one rectifier circuit in a unit, it structure is very simple. These

advantages are suitable for the MAV-installed system. However, the disadvantage is the design; the completely SPFA has not been reported. Therefore, I surveyed the SPFA design based on patch antenna for circular polarized wave (ACPW) in Figure3.20

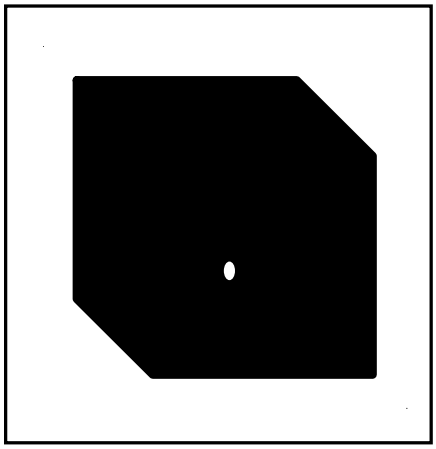

Figure 3.20 Pattern of Patch Antenna for Circular Polarized Wave

Chapter 4
Experimental Devices

This chapter shows the power transmission system, the power receiving system the demonstration and others for the experiments.

4.1. Power Transmission System

4.1.1 System overview

Figure4.1 shows the block diagram of the transmitting system. Microwaves generated by the 5.8-GHz oscillator are divided into five by the 8-ways power divider. And then each of them is added phase shift by the phase shifter. The amount of shifted phase is controlled by software. After phase shifting, their power levels are amplified by two steps, driver amplifiers and power amplifiers. Finally the microwaves with enough power level are radiated into the free space through the horn antennas.

Figure 4.1 System overview

Table 4.1 Specifications of Phased Array Antenna

Parameters	values
microwave frequency	5.8GHz
wavelength, λ	51.7mm
total transmission power, P	3.5W
array pitch, d	110mm (d/λ=2)
steering angle, θst	9deg
divergence angle, θd	6deg
diameter of the array, D	330 mm

4.1.2 Oscillator

Figure4.2. shows the oscillator “ArumoTech-OS00T2182” and Table shows its specifications. This oscillator is composed of plate-tuning method and Metal Oxide Semiconductor Field Effect Transistor (MOSFET). The output power is stable and about 10 dBm.

Figure 4.2 Oscillator

4.1.3 Power divider

Figure4.3 shows the 8-ways power divider “ArumoTech-PD00T2301”. At this power divider, the microwaves from the oscillator are divided into eight, which become about 1.25 mW. In this study, only five ports were used and the others of three ports were terminated with 50-ohm terminators.

Figure 4.3 Power divider

4.1.4 Digital phase-shifter

Figure4.4 shows the digital phase shifter “ArumoTech-FS01T2150”. This phase shifter is digitally controlled by 6-bit signals from a computer. And its phase resolutions are found to be $360/2^6 = 5.625, \deg$. For example, the signal of “010101” in binary becomes 118.125 deg of phase shift. Table shows the specifications of these four phase shifters.

This phase shifting mechanism is represented in Fig. The phase shifter digitally switches the transmission lines to change the physical length. As a result this phase shifter can shift the microwave phases.

Figure 4.4 Digital phase-shifter

4.1.5 Driver amplifier

Figure4.5 shows the driver amplifier “ArumoTech-AP01T2149”. This driver amplifier amplifies the microwave power level after the phase shifters to compensate the power loss by the phase shifters.

Figure 4.5 Driver amplifier

4.1.6 Power amplifier

Figure4.6 shows the power amplifier “ArumoTech-OS00T2182”. This amplifier is FET based type and boosts the microwave power to the desired level of 0.7 W. The sum of these five power amplifier outputs was about 3.4 W, which we regarded as output power from transmitting system. Table shows the specifications of these power amplifiers.

The power amplifiers generated heat from the heavily-loaded FET, and then this heat caused the

power down and instability of the transmitting system. Because the cooling fins installed on these power amplifiers did not seem so enough, we installed the CPU fans over these power amplifiers for air cooling.

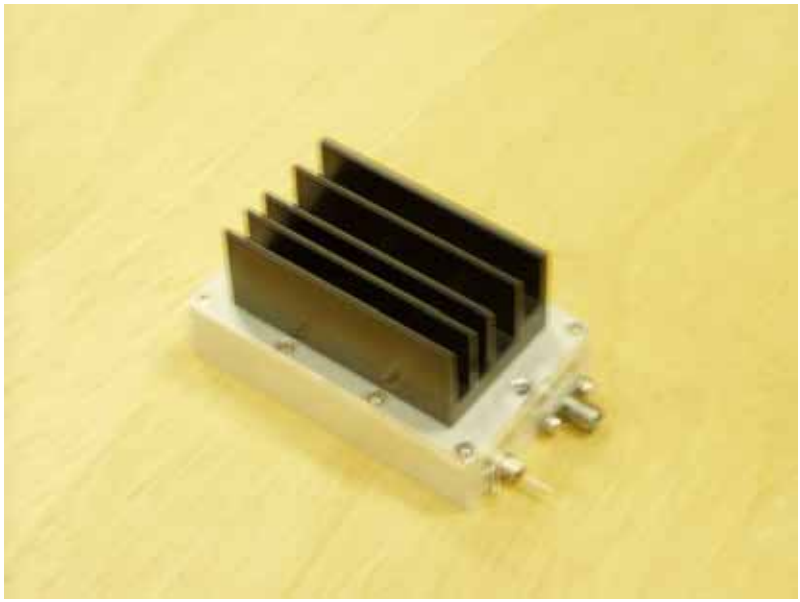

Figure 4.6 Power amplifier

4.1.7 Booster amplifier

Figure4.7 shows the booster amplifier “ArumoTech-AP00T2388”. This amplifier boosted the microwave power level by 4.5 dB between the oscillator and power divider. Without this booster amplifier, the final output power often fluctuates due to the changing power loss by the phase shifters. Then this amplifier boosted the power level before the divider and saturated it after the power amplifiers. Consequently this booster amplifier can stabilize the final output power level.

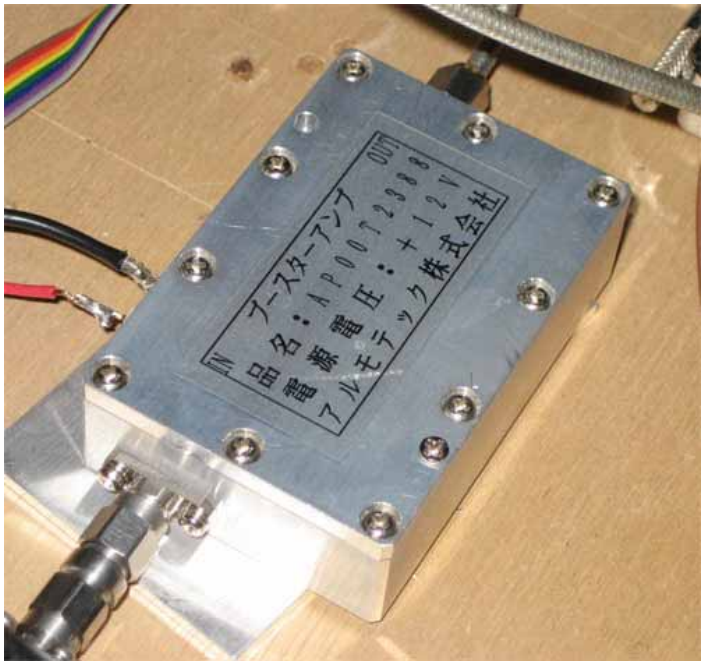

Figure 4.7 Booster amplifier

4.1.8 Horn antenna

Figure4.8 shows the picture of the horn antenna and Fig. represents the dimension of this horn antenna. The horn antenna is fine at its sharp directivity characteristics and high gain. So this antenna seems easy to be controlled and effective for a phased array element. The radiation field theory will be described in Ch.3.

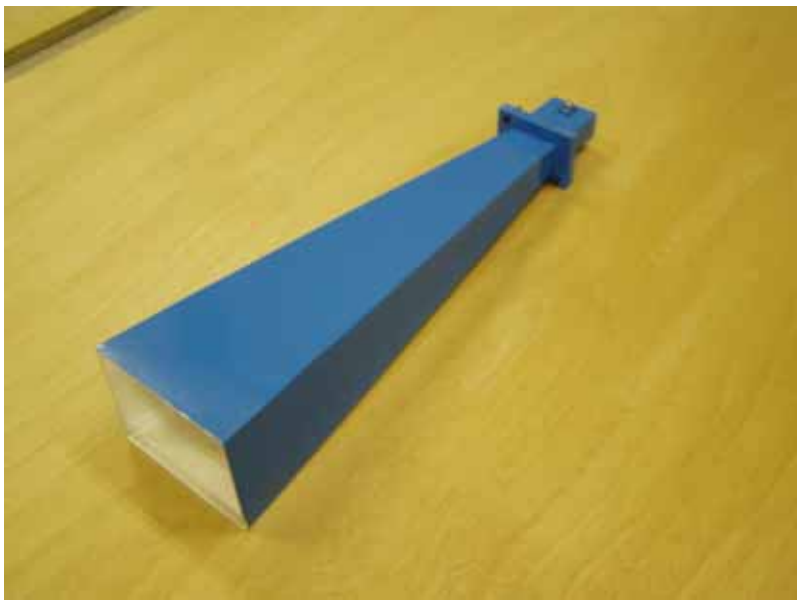

Figure 4.8 Horn antenna

4.2. Power Receiving System / Measurement Apparatus

Figure4.9 shows the power receiving system. It composed of antennas, rectifiers, an open/load switching unit and an oscilloscope. The microwave transmitted by the power transmitting system was received by the antennas, and was converted to DC power by the rectifiers, and was loaded by the open/load switching unit and was measured as the output voltage by the oscilloscope.

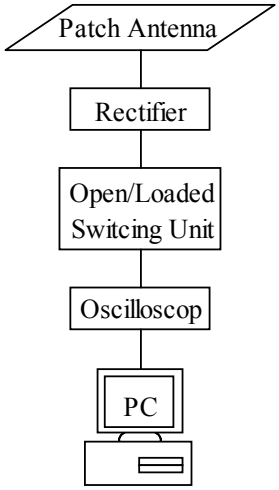

Figure 4.9 Schematic of Power Receiving System

4.2.1 Patch antenna

Figure4.10 shows a patch antenna (ArumoTech). We used it as a standard receiving antenna. Its shape was a rectangle and its characteristic impedance was matched in 50Ω.

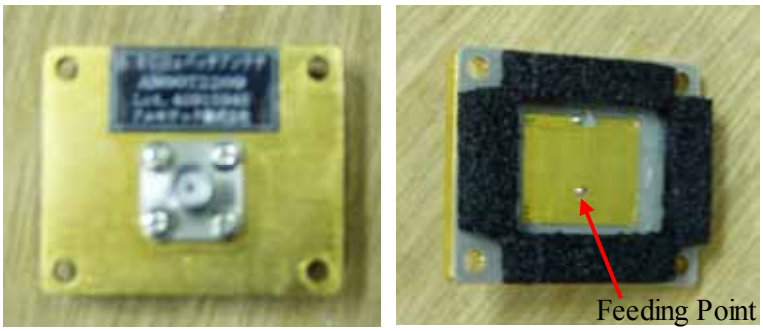

a) Rear b) Front

Figure 4.10 Picture of Patch Antenna

4.2.2 Rectifier

Figure4.11 shows a rectifier (Pasternack Enterprises, Inc.-PE8016). We used it as a standard rectifier. Figure4.12 shows the characteristic of the rectifier; the relationship between the input power P_{in} and the output voltage V_{out}. The curve in this graph was the fitted curve of this relationship and the input power P_{in} was calculated back with the output voltage V_{out} by:

$$P_{in} = 1.8166 \times 10^{-8} \cdot {V_{out}}^3 - 1.4833 \times 10^{-5} \cdot {V_{out}}^2 + 1.2969 \times 10^{-2} \cdot V_{out} \quad (4.1)$$

Figure4.11 Picture of Rectifier

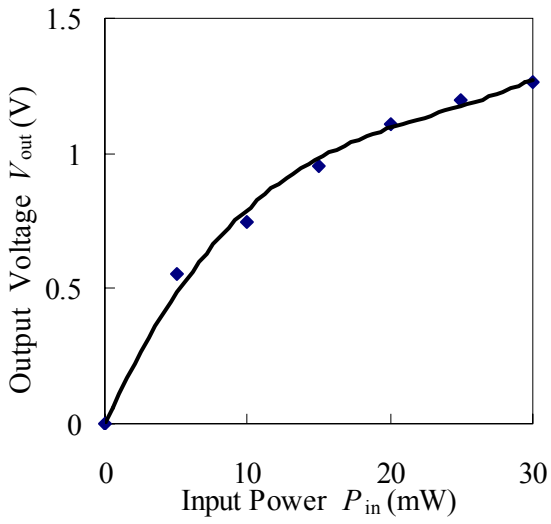

Figure 4.12 Characteristic of Rectifier

4.2.3 Open/Load switching unit

Figure4.13 shows a open/load switching unit, and Figure4.14 shows the schematics of the device. It installed after the rectifier and before the oscilloscope. It was able to switch between the open circuit mode and the loaded circuit mode. It had an analog linearly-variable resistance element in the range 2-4500Ω. We were able to measure the open output voltage V_o in the open circuit mode (Figure4.14a)), and the loaded output voltage V_L and the Voltage V_i for calculating the current in the loaded circuit mode (Figure4.14b)).

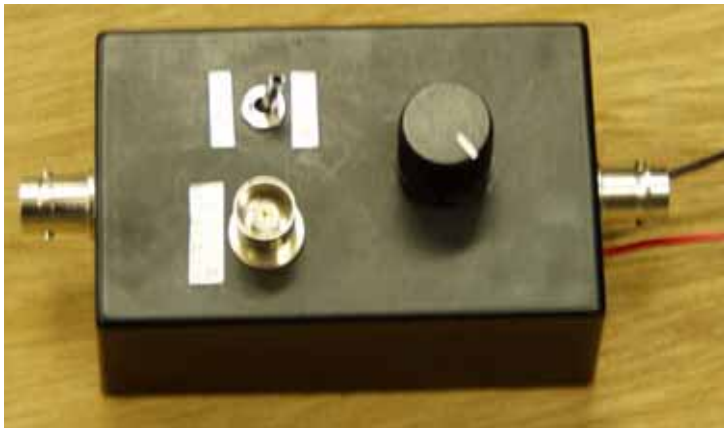

Figure 4.13 Picture of Open/Load Switching Unit

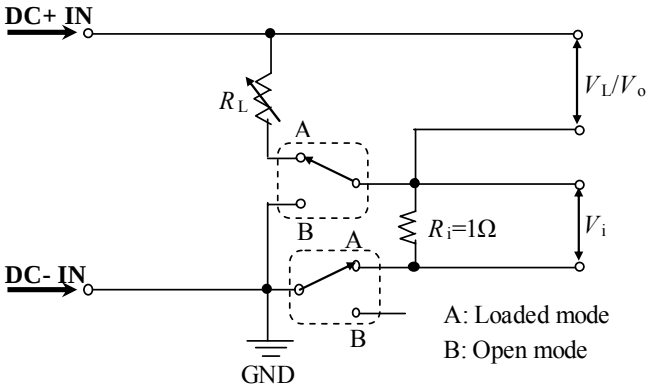

a) Circuit Schematic

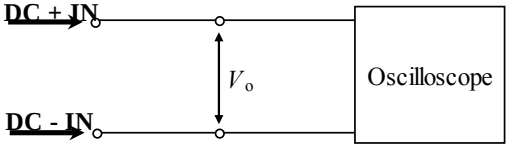

b) Open circuit

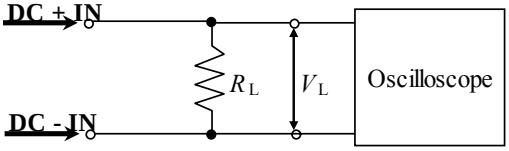

c) Loaded circuit

Figure 4.14 Schematics of Load/Open Switching Unit

4.2.4 Oscilloscope

Figure4.15 shows oscilloscopes (Keyence-NR-2000, Keyence-NR-110). Although we measured the data with NR-2000 in the early phase of our experiment, we replaced it by NR-110 in the later phase due to circumstances beyond our control. Table4.2 shows the specifications of the oscilloscopes. It measured the output voltage from the rectifier and sent the data to a computer for saving and analyzing.

a) NR-2000 (Keyence) b) NR-110 (Keyence)

Figure 4.15 Pictures of Oscilloscopes

Table 4.2 Specifications of Oscilloscopes

Model Name	NR-2000	NR-110
Ch.	16ch(Single), 8ch(Differential)	16ch(Single), 8ch(Differential)
Resolution [bit]	14	14
Range [V]	10, 5, 2.5, 1, 0.5, 0.25	10, 5, 2.5
Gain	x1	x1 / x10
Input Impedance [MΩ]	1 (±1%)	1 ~
Max. Sampling Freq. [kHz]	400	50
PC Interface	USB 1.0 ~	PCMCIA2.1 / JEIDA4.2 ~

4.2.5 Attenuator

Figure2.16. shows the attenuator “Pasternack Enterprises, Inc.-PE7165-5” which adjusts output power range from 0dB to 20dB.

Figure 4.16 Attenuator

4.2.6 Power Meter

Figure2.17 shows the power meter “BOONTON POWER METER2061016” for to measure high frequency wave power.

Figure 4.17 Power Meter

4.2.7 Polarity-Free Leaf-Patch antenna

Figure 4.18 shows Polarity-Free Leaf-Patch antenna which is made in this Lab. It has about 40% (Table 4.3) conversion efficiency making RF from out of rectifier to in. In a word, it can receive 40% of the energy unit area from the horn antenna in any yaw angle. In this paper, all the efficiency calculations consider 40%.

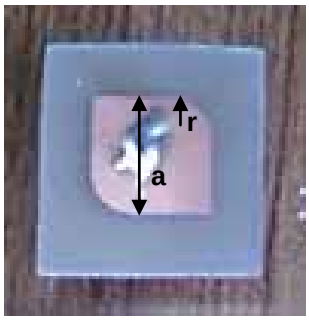

Figure 4.18 Polarity-Free Leaf-Patch antenna

Table 4.3 Specifications of Polarity-Free MSA

(a) Efficiency of Leaf antenna

Antenna Pattern	Leaf type
Chamfering Ratio r/a	0.33
Average	40%
Max.	44%
Min.	36%

(b) Input power in Leaf antenna

Distance from horn antenna, cm	Input power, mW/個
22	12.7
42	6.2
62	2.4
82	1.8
102	1.2

4.3 Experimental Setup and Others

I measured on a mounting structure surrounded by flat tile ferrite absorber. Additionally, I made rectenna elements of glass-epoxy substrate. In this section, I describe about the mounting structure and others for experimenting or demonstrating.

4.3.1 Mounting structure

Figure4.18 shows a mounting structure for the receiving modules. It was made of wood and thermoplastics. It consisted of a large wooden framework and a traverse stage enabling the receiving modules to slide smoothly in the y-axis direction. The framework was surrounded by flat tile ferrite absorber for reducing the reflection effect. The mounting structure was designed to make measurements in Cartesian coordinates. It allowed for continuous movement in the y-axis and discrete step movement in the other two axes. The movable ranges were: x: ±290(mm), y: ± 400(mm), z: 235 + 100n (mm) <n = [0, 11]>.

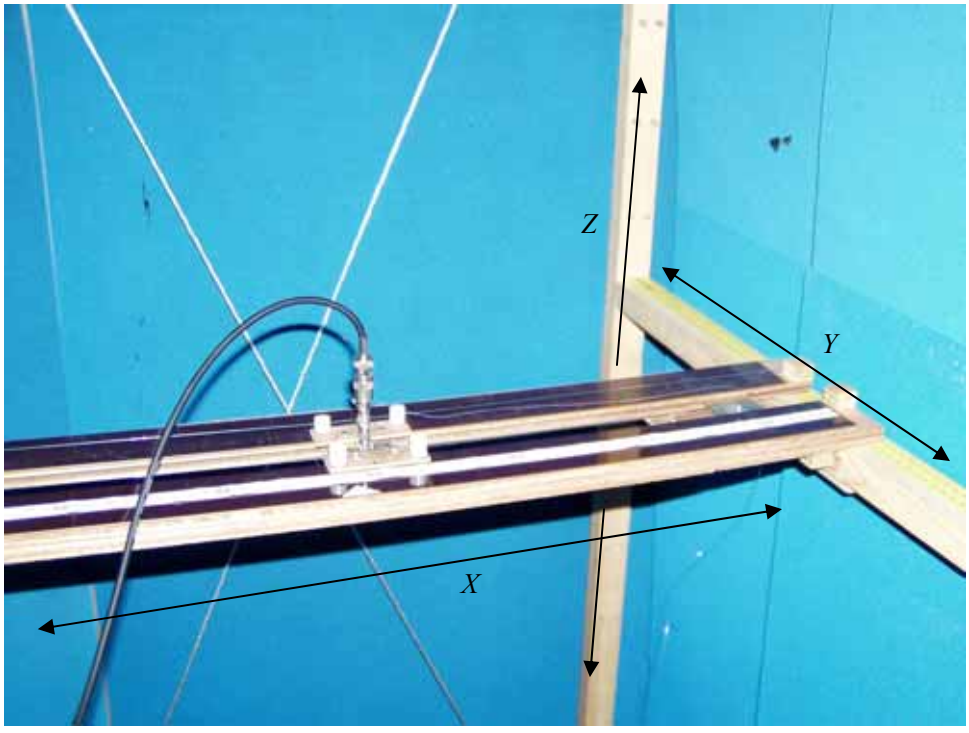

Figure 4.18 Picture of Mounting Structure

4.3.2 Substrate

In the experiments, I used glass-epoxy substrate FR-4 (Sanhayato Corp.). Table4.4 shows the specification. We used its dielectric constant of 4.7 and its dielectric dissipation factor for calculation of 0.020. The substrate was pre-coated with photosensitive paint and left the antenna-patterns coating by developing. Then the unnecessary cupper area was removed by substrate etching.

Table 4.4 Specification of Substratum

Material	Glass-Epoxy (FR-4)
Dielectric Constant ε_r	4.5~4.8 (1MHz)
Dielectric Dissipation Factor $\tan\delta$	0.015~0.020 (1MHz)
Dielectric Thickness h [mm]	1.6
Conductor Thickness t [μm]	35

4.4 Demonstration

4.4.1 Electrical Motor

Figure4.19 shows a electrical motor for the power transmission demonstration and Table4.5 is its specification. Although It was installed the AERO SOARER (TOMY Company Ltd.), the manufacture was not identified. Since it was able to operate with low electric power, I adopted it for the demonstration.

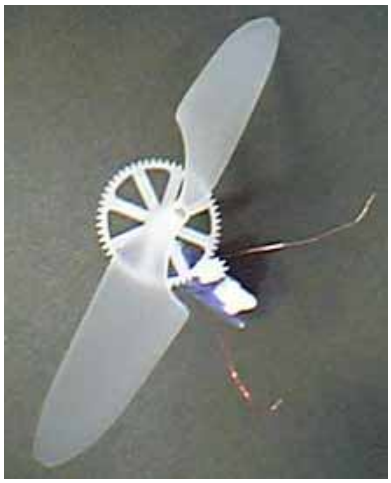

Figure 4.19 Picture of Electrical Motor

Table 4.5 Specification of Electrical Motor

Size	Glass-Epoxy (FR-4)
Min. Operating Voltage V_{min} [mV]	200
Min. Operating Current I_{min} [mA]	6
Inertial Resistance R_L [Ω]	33
Rated Voltage V_{rat} [V]	2.0
Rated Current I_{rat} [mA]	60

4.4.2 Fixed base

Figure 4.20 shows fixed base which is installed switching point and Model of airplane as MAV for the demonstration. Figure 20 shows schematic of this system.

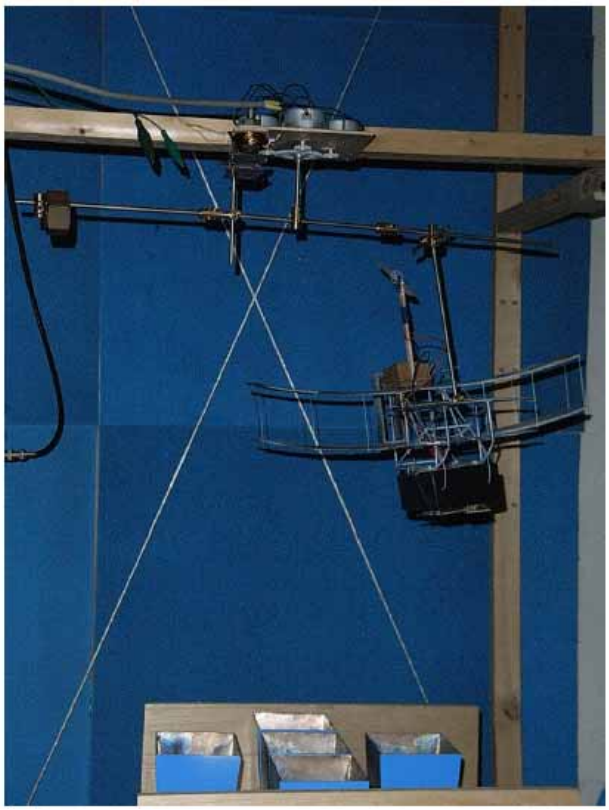

Figure 4.20 Fixed base for demonstration

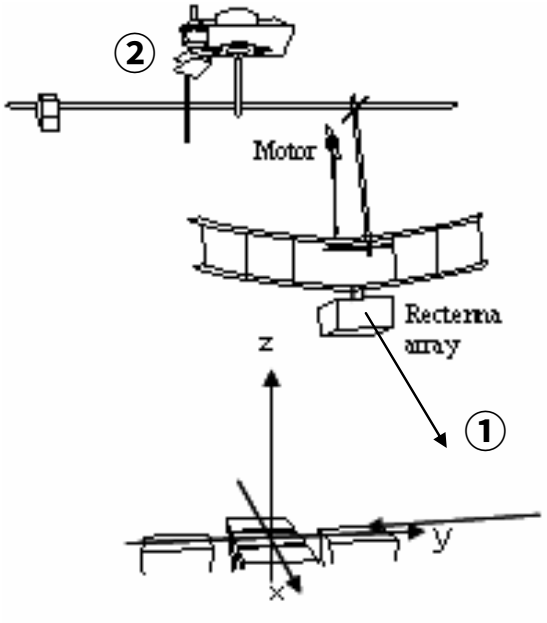

① To measurement system
② Rotating switching point

Figure 4.21 Schematic of demonstration method

Chapter 5
Experiment Results and Discussion

This Chapter shows the measurements results of the experiments and discussions about the rectifier circuit patterns, rectennas array and demonstration. This is the main part of this paper.

5.1 Rectifier circuit design

5.1.1 Schematic of the rectifier circuit

The rectifier circuit of a general rectenna is made up of figure 5.1. It has big enough capacitance in the line and it is understood theoretically to obtain the conversion efficiency of 100%. I paid attention to the parameter that composed the rectification circuit. And, it thought making the rectification circuit suitable for needs, and making it to highly effective. Table 5.1 shows standard parameters of the rectifier circuit.

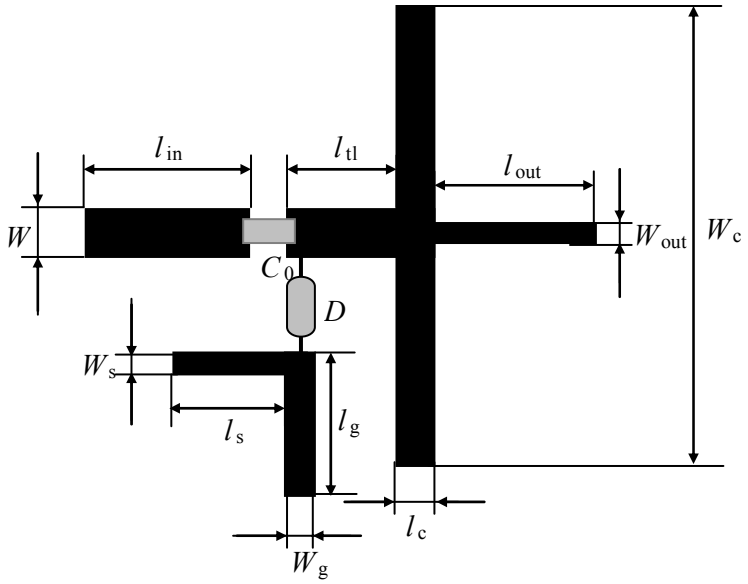

Figure 5.1 Schematic of Rectifier Circuit Pattern Parameters

In designing rectifier circuit patterns, variable parameters are below:

- Type of Schottky Barrier Diode (SBD): D
- Capacitance of chip condenser: C_0
- Input width: W
- Input length: l_{in}
- Width between diode and ground: W_g
- Length between diode and ground: l_g
- Stub width after diode: W_S
- Stub length after diode: l_S
- Output transmission line (OTL) length: l_{tl}
- Low Pass Filter (LPF) shape: W_C, l_C
- Output width: W_{out}
- Output length: l_{out}

Table 5.1 Parameters for Standard Rectifier Circuit Pattern

Parameters	Value / Product
D	1SS97 (NEC)
C_0 [pF]	33 (muRata-GRM42-6 SL 330J 50)
W [mm]	2.53
l_{in} [mm]	10.00
W_g [mm]	1.50
l_g [mm]	8.20
W_S [mm]	1.00
l_S [mm]	0
l_{tl} [mm]	10.00
W_C [mm]	28.00
l_C [mm]	2.00
W_{out} [mm]	1.00
l_{out} [mm]	10.00

Figure5.1 shows their parameters on the pattern. The parameters of W, l_{tl} are predetermined by the theory; W=2.83mm at 5.8GHz for impedance matching, and $l_{tl}=\lambda_g/4$ for output filter. Moreover, it was founded by the research in the Kyoto University that some parameters seldom affect the conversion efficiency; C_0, l_{in}, W_g, W_S, W_C, l_C, W_{out} and l_{out}. First I designed the standard rectifier circuit patterns. Table5.1 shows its values and products. I experimented with varying the parameters independently and discuss the results below.

In following experiments, I connected the test rectifier circuit to the oscillator directly, and I measured the output voltage $V_{measured}$ from the rectifier circuit with the oscilloscope. The wattage $P_{measured}$ of the load is expressed as:

$$P_{measured} = \frac{V_{measured}^2}{R_L} \tag{5.1}$$

where R_L is the resistance value of the load. Since the input power P_{in} is given as 10dBm from the oscillator specification, the conversion efficiency of the rectifier circuit is found by:

$$\eta = \frac{P_{measured}}{P_{in}} \tag{5.2}$$

Thus, I calculated the efficiencies with changing the parameters.

The width of the input line W and length l_{in} are parameters decided by the characteristic impedance 50Ω. The value at this time is respectively as shown in the table 5.1.

Generally, when the load is connected to the output terminal of a transmission line, the input impedance of the transmission line is expressed as:

$$Z_{in} = Z_0 \frac{Z_L + jZ_0 \tan \beta l}{Z_0 + jZ_L \tan \beta l} \tag{5.3}$$

where Z_0 and Z_L are the characteristic impedances of the transmission line and the load, and β is the phase constant. When the line length is integer multiples of $\lambda_g/2$, or even multiples of $\lambda_g/4$, $\beta l = (2\pi / \lambda_g) \cdot (2n\lambda_g / 4) = n\pi$ (n is an integer of 0 and over), and (5.4) is represented as:

$$Z_{in} = Z_L \tag{5.4}$$

It means the input impedance is equal to Z_L when the line length is $n\lambda_g/2$.

When the line length is odd multiples of $\lambda_g/4$, $\beta l = (2\pi / \lambda_g) \cdot \lfloor (2n+1)\lambda_g / 4 \rfloor = (2n+1)\pi / 2$, $\tan \beta l = \infty$, and (5.3) is represented as:

$$Z_{in} = Z_0^2 / Z_L \tag{5.5}$$

It means that the relationship between Z_0 and Z_L is the inversion.

I paid attention and try to improve to the capacitor of the input filter and the capacitor part which is composed the MSL of the output filter, C_0, l_c, W_c and part of the stub, l_s.

5.1.2 Experiment method

Figure5.2 shows diagram of the experiment method. Each device is explained details in Chapter 4. First, Oscillator is making 5.8GHz microwave, attenuator adjust this wave, rectifier make this wave rectify considering load resistance, and detect output power or voltage in the PC.

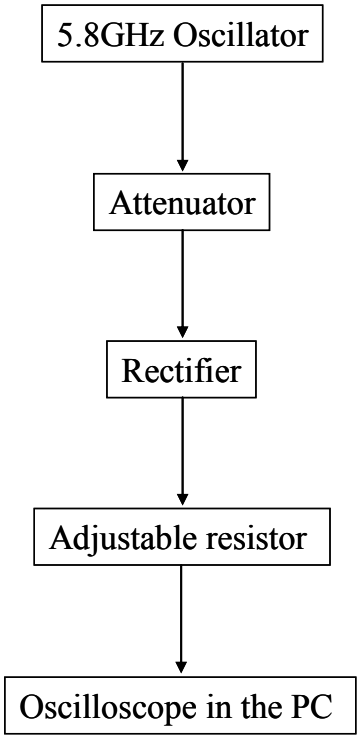

Figure 5.2 Diagram of the experiment method

5.1.3 Stub Length: l_s

In the research by the University of Kyoto, the stub after diode was theoretically necessary because there is AC effect before and after diode. That was founded that there remained some AC effects. For remove the effects, the stub was needed as a filter. However, in this experiment in the University of Tokyo, Figure5.3 shows the result. As a result, although the length was one of the effective parameters, it was unnecessary in my rectifier circuit (l_S=0).

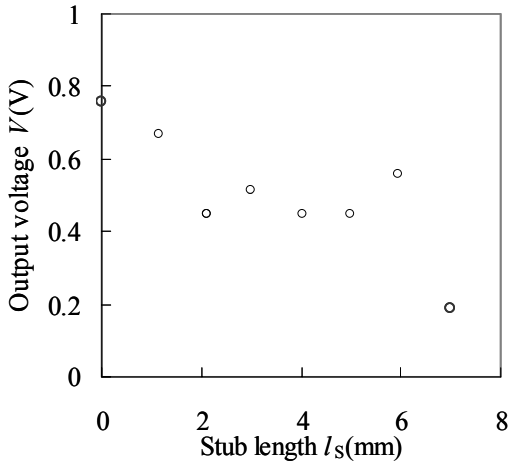

Figure 5.3 Relationship between Stub Length and Output Voltage

5.1.4 Low Pass Filter: W_C and l_C

Figure 5.4 shows the result. W_C and l_C are the width and the length of the output LPF. Its equivalent circuit is a condenser connected in parallel, and its capacitance can be found by the equations (3.16-18). From the equations, the standard LPF capacitance C_{eq_std} was about 1.53pF, and it was enough large to smooth output DC and to filter the reminded AC. For observing the effects of the LPF shape, I designed another LPF shape; W_C=20mm, l_C=3mm, and C_{eq}=1.03pF.

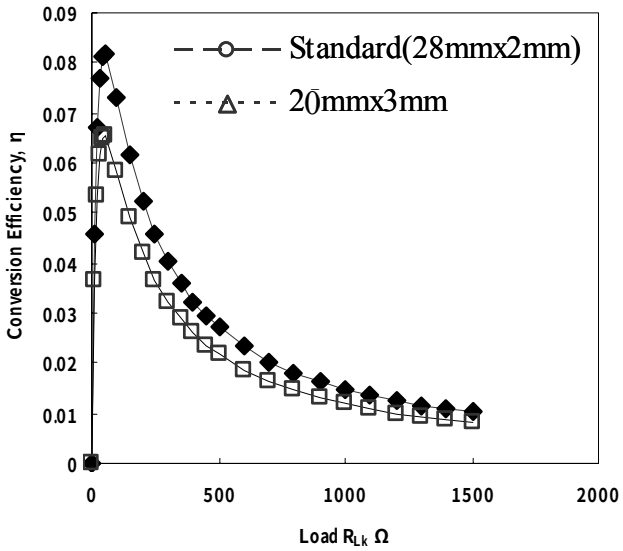

Figure 5.4 Load Characteristic related to LPF shape

5.1.5 Capacitance of Chip Condenser: C_0

It is difficult to express the capacitor of the series connection on MSL. Then, it use chip condenser on MSL. Each inductance as;

$$X_c = \frac{1}{\omega C} \qquad (5.6)$$
$$X_L = \omega L$$

In theory, chip condenser has small capacitance is matching high frequency wave circuit like eq(5.6). However, I changed variety capacitance of chip condenser (muRata-GRM42-6 series) on the rectifier, and measured conversion efficiency. Table 5.2 shows the result. As a result, 100pF is most high efficiency at the 260Ω in this rectifier.

Table 5.2 Efficiency of Chip Condenser

Capacitance (pF)	Load resistance (Ω)	Efficiency (%)
5	260	16.2
10	260	8.3
30	260	21.7
50	260	15
100	260	33.7
150	240	26.9
470	260	24.1

5.1.6 Efficiency of New Rectifier Circuit

I redesigned the rectifier circuit. Table5.3 shows the redesigned parameters, based on the above results. Figure5.5 (Sample average value, Number of sample : 3 each one, Range of error : ～± 8%) shows the effect of redesigning. As a result, the conversion efficiency is growing up at the input power 10mW. It takes 34% conversion efficiency RF-DC at the 250Ω load resistance. Generally, the conversion efficiency changes by the load resistance and the input electric power. It actually seems that the conversion efficiency rises in addition by taking the impedance matching this time. However, it will be much higher efficiency than this time by taking between the impedance matching and the load resistance. Figure 5.6 shows that result. From this, maximum efficiency is 49%, input power 700mW at the 250Ω.

Table 5.3 New Rectifier Parameters

Parameters	Value / Product
D	HSM88WA
C_0 [pF]	100 (muRata-GRM42-6 SL 1000J 50)
W [mm]	2.53
l_{in} [mm]	**10.00**
W_g [mm]	**1.50**
l_g [mm]	**8.20**
W_S [mm]	**1.00**
l_S [mm]	**0**
l_{tl} [mm]	10.00
W_C [mm]	20.00
l_C [mm]	3.00
W_{out} [mm]	**1.00**
l_{out} [mm]	**10.00**

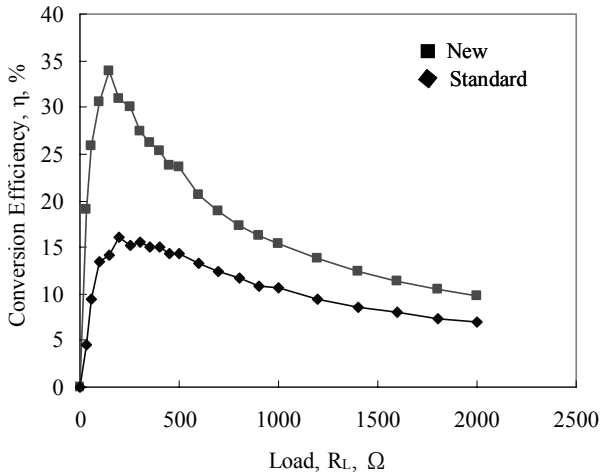

Figure 5.5 Conversion of efficiency

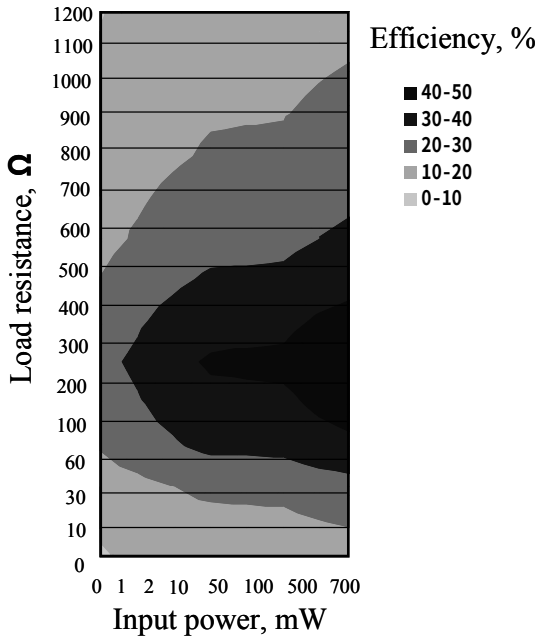

Figure 5.6 Contour map of the rectification efficiency

5.2 Rectennas Array

5.2.1 Rectenna

Here, the rectifier circuit is compared with the conversion efficiency when making it to Rectenna. The measurement method shows Figure 5.7. The relation between the input electric power and height (distance from transmission antennas) is described 5.2.4. Figure 5.8 (Input power 10mW, Sample average value, Number of sample : 5 each one, Range of error : ～±5%) shows the result. The characteristic is almost corresponding as figure 5.8 shows. The maximum conversion efficiency changed because the entire load resistance increased by the antenna. Rectenna takes 33% conversion efficiency RF-DC at the 260Ω. It seems to be safe even if the data of rectenna the measurement data is the data of rectifier the measurement.

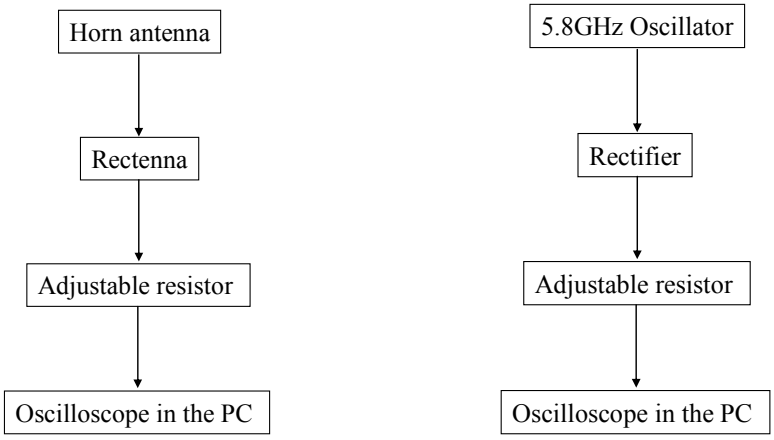

(a) The measurement recntenna (b) The measurement rectifier

Figure 5.7 The mesurement method diagram

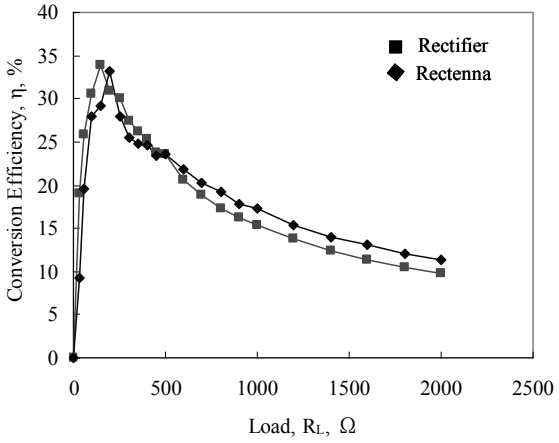

Figure 5.8 Conversion of efficiency, Rectifier and Rectenna

5.2.2 Making series and parallel array

It is necessary to know the characteristic when the rectenna is made parallel or series to obtain the electric power for moving the motor of MAV (in detail Chapter 4). At this time, if making to the series and making to the parallel match it well in the rectennas array, the voltage and the current can be added. Figure 5.9 shows the measurement method. Two recntennas shows 5.2.1 use this experiment. One rectenna obtain the power, P_{1max}, another recntenna obtain the power, P_{2max} , rectennas array obtain the power, P_{cmax}, then power drop defines;

$$Power\ drop = \frac{(P_{1max} + P_{2max}) - P_{cmax}}{P_{1max} + P_{2max}} \tag{5.7}$$

Table 5.4 shows result. According to result, the electric power has decreased in making of the rectenna series. This can be to obtain the voltage will have decreased. Oppositely, when the rectenna is made parallel, obtained electric powers are almost two times. This is because the current can be added. As for the phenomenon of the electric power decreased, it is possible that the conversion efficiency shifts from the best point by making to rectenna array like figure 5.8. From above result, the current can be added by making the rectennas parallel array.

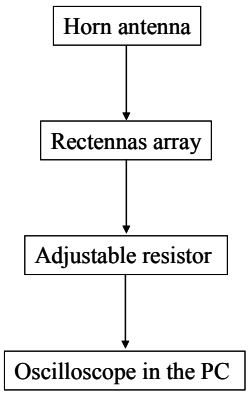

Figure5.9 The mesurement method diagram

Table 5.4 Efficiency of series and parallel array

	Series	Parallel
H(cm)	power drop(%)	power drop(%)
—	52	9.4
42	50.3	12.4
62	49.2	9.1
82	49.6	10.3

5.2.3 Making Parallel Rectennas Array Consolidate and Compact

As for the power transmission energy is characterized to Gaussian distribution, and the energy density of center part is higher in shown chapter2. I improve the efficiency of receiving the power transmission energy by making the rectifier and the antenna vertical as shown in figure 5.10. Figure 5.11 shows that arrangement of antenna in energy distribution at the 102cm from transmission antennas. According to the Gaussian distribution

$$\pi / (1\text{-}1/e) = 4.97 \tag{5.8}$$

The center part is higher 4.97 times than the mean value. It is easy to understand from eq (5.8). In theory, arrangement rentennas array in the center part makes receiving energy increase. At this time, table 5.5 shows this result. According to result, it improved more 10% receiving the power. In addition, it is thought that this difference is remarkably in a high point with more rectennas.

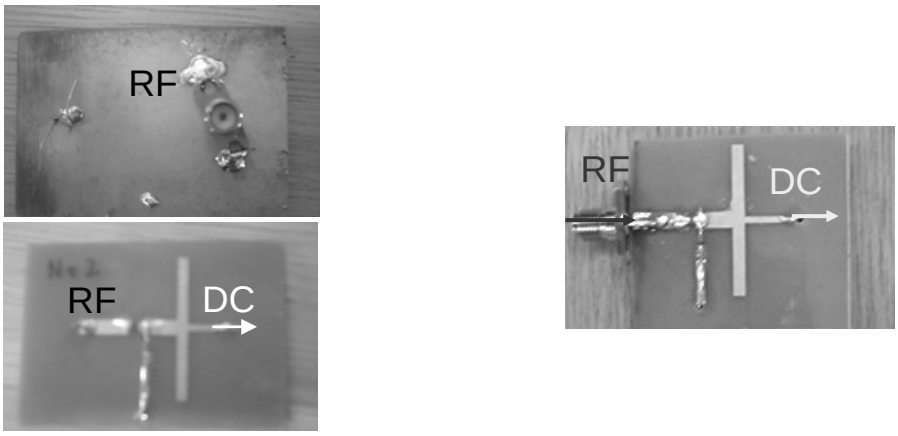

(a) Existing (b) Vertical

Figure 5.10 Energy intensive of rectennas

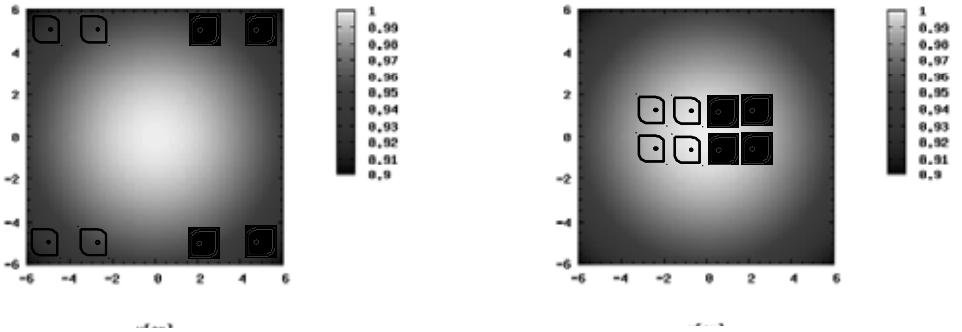

(a) Existing (b) Intensive

Figure 5.11 Arrangement of recntennas

Table 5.5 Energy rate of increase

Number of Rectenna	The rate of increase, %
8	11.05
16	13.55
32	22.66
64	36.93

5.2.4 Making New Rectennas Array

The new recntennas array is made based on the above-mentioned result. Connecting eight rectennas array in parallel make the motor of MAV correspond with load resistance, because the motor of MAV of load is 33Ω, the maximum conversion efficiency of rectenna takes 33% at the 260Ω. I designed new rectennas array like figure 5.12. Figure 5.13 shows available for receiving electric power each unit area and in theory outside diameter of energy (in detail chapter2, chapter3 and chapter4). According to this result and figure 5.6, one rectena can receive power 1.2mW at the 102cm, 24%, 1.8mW at the 82cm, 29% with using this eight rectennas array.

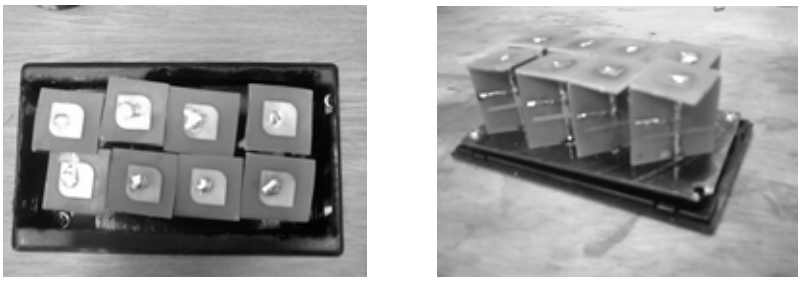

Figure 5.12 New rectennas array

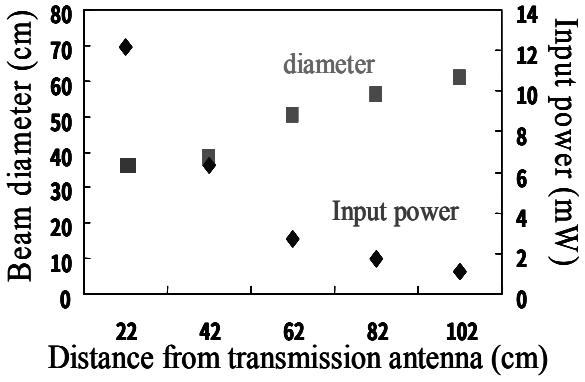

Figure 5.13 Beam diameter and input power

Figure 5.14 shows the conversion efficiency and output voltage of one recntenna each at the 82cm and 102cm. It needs 200mV per one rectenna to move the motor of MAV because of not add voltage in series array. This result gives me that I can move the motor of MAV at the 82cm. At this time figure 5.15 shows that I measured like figure 5.9 the characteristic of new rectennas array. According to this result, at the 33Ω it achieved about 250mV, 7.97mA,1.99mW. This is enough power to start the motor of MAV. It can explain the decrease phenomenon from 5.2.3, not impedance matching, radiation, reflection from substrate glass-epoxy and so on.

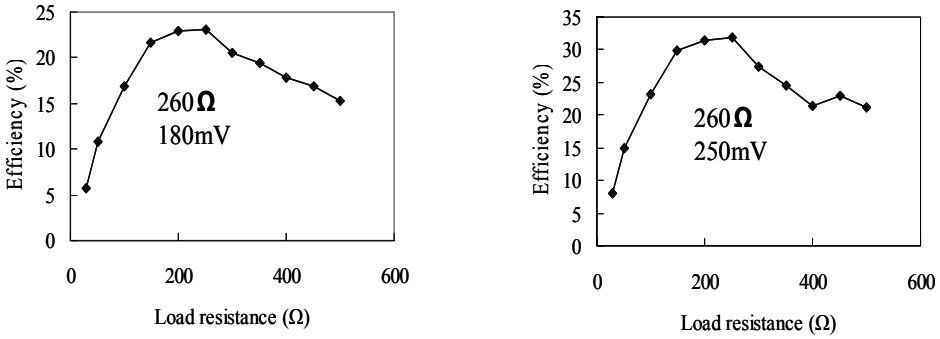

(a) 102cm from horn antenna (b) 82cm from horn antenna

Figure 5.14 Conversion efficiency and output voltage

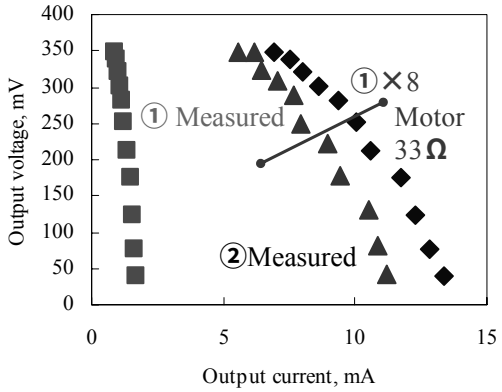

(a) ① Measurement efficiency of 1 rectenna
(b) ② Measurement efficiency of 8 renctennas

Figure 5.15 Characteristic of new rectennas array, 82cm from horn antenna

5.3 Demonstration

All experiment method in this paragraph is shown as chapter4.

5.3.1 Beam steering

Its theory in detail is shown as chapter2. Figure 5.16 shows that the result of MAV installs and is fixed the rectennas array in Y-axis 9deg steering the energy beam from Z-axis at the 82cm from horn antenna. According to this result, only MAV can receive power from horn antenna, it can move. Because output voltage got out-perform 200mV. The lobe of another energy is grating lobe. This is feature of high frequency wave. Figure 5.17 shows X-axis 9deg steering the energy beam from Z-axis at the 82cm from horn antenna. This is the result by the same reason token. This result shows beam steering can continue to function normally.

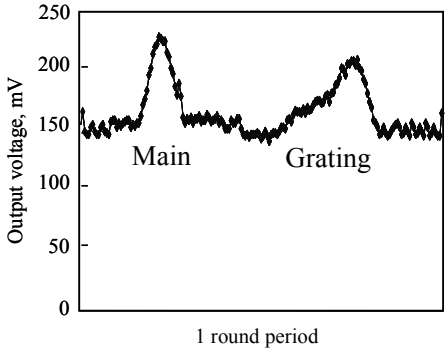

Figure 5.16 Y-axis output voltage per 1 round

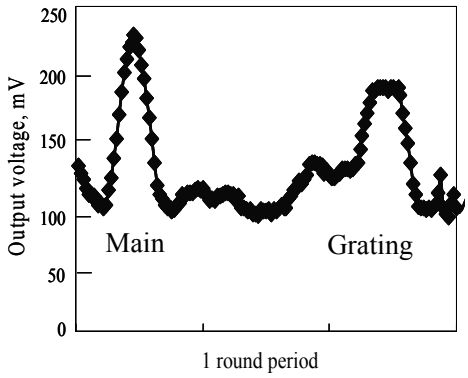

Figure 5.17 X-axis output voltage per 1 round

5.3.2 Beam synchronized with MAV

I tried the synchronization of the beam and MAV. The program I made of using Lab-view has performance the according to MAV rotated at a constant speed makes the energy transmission system be able to able to begin transmit beam when MAV passed through the switching point. Figure 5.18 shows this result. According to it, MAV can obtain enough power to move the motor over 1 round. This shows that MAV was available as the transmission energy.

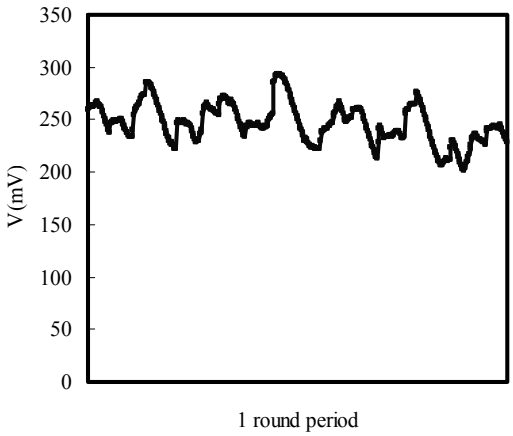

Figure 5.18 Synchronized result of the output voltage per 1 round

Chapter 6
Conclusions

This Chapter shows the conclusions of my study, and describes future vision.

6.1. Conclusions

- I reviewed the parameter of the rectifier circuit, and I choose that have made improve the best value from the experiment result. The quality of rectifier used in this rectennas array came to be able to convert input-RF into output-DC at the maximum 49% in the 700mW input.
- To obtain the energy beam efficiency, by making the antennas-intensive parallel array. In the 82cm this energy field, I developed the rectennas array with the maximum conversion efficiency of 33% at the load resistance of 260Ω.
- I established the system by synchronized the motor of rotating MAV with the steering power transmission energy from horn antenna. The high conversion efficiency of renctennas array made that possible.

6.2. Future vision

Through my study, I established the system by synchronized the motor of rotating MAV with the steering power transmission energy from horn antenna. In addition to this, target tracking system is needed. To establish the target tracking software retro-directive system (chapter1), it needs to confirm operating accuracy in the same distance from the transmission antenna to MAV, more 82cm.

Firstly, it needs to apply the system not to confuse the microwave from transmission antenna with the microwave. However, the frequency band is too different will make it become poor system generality. It needs to consider it to read for consistency and where place an emphasis.

Secondly, highly-reproducible is required. Because antennas used in the target tracking system is hand-made, to reflect the output-voltage from it in the equipment accurately. For that, I consider it the rectifier for the target tracking system is more important than its conversion efficiency.

Finally, it which type of antenna, arrangement of antenna, frequency and so on is decided after due consideration from the experimental results and theory. I hope all systems work accurately and achieve “Microwave energy transmission to the MAV” in the near future to take advantage of my study.